Investigation into the Interactions of Supercritical Argon as a Solvent with trans-1,2-dichloroethylene Using Ultraviolet-Visible and Infrared Spectroscopy

A thesis presented in partial fulfilment of the requirements for the degree of

Masters of Science

in

Chemistry

at Massey University, Auckland, New Zealand.

Erin Sarah Moffet

2018

Abstract

This thesis looks at the uses and interactions of argon as a solvent at or above its supercritical temperature and pressure. A supercritical fluid allows for a range of properties depending on where the conditions of pressure and temperature are in relation to the critical point of the chosen substance. These supercritical fluids have been shown to be useful across many areas of industry and research and are the ideal fluid to use in a molecular beam pulsed valve.

Solubility interactions of argon and trans-1,2-dichloroethylene (DCE) across multiple conditions were monitored using ultraviolet-visible (UV-Vis) and infrared (IR) spectroscopy. Two high pressure cells were designed, constructed and tested to withstand the 50 atmospheres and 140 K conditions required. The initial cell focused on UV-Vis spectroscopy with the DCE vapour showing an exponential decrease in absorbance as the temperature in the cell was reduced. Changing conditions to reach the supercritical region of argon resulted in a significant increase in the absorbance and therefore the solubility of DCE.

The second cell constructed focuses on analysis using infrared spectroscopy and showed clear peak shifts and shape changes at the b_u CH stretch (ν_9) and b_u CH bend (ν_{10}) for trans-1,2-dichloroethylene (DCE) The intensity at a_u CH bend (ν_6) and b_u CCl stretch (ν_{11}) proved to be less informative. DCE vapour acted predictably as the temperature was reduced, resulting in a significant drop off in absorbance similar to that observed in the UV-Vis. In changing to the supercritical and liquid argon conditions resulted in the appearance of an

asymmetric lineshape characteristic of Fano resonance, which is not common in infrared spectroscopy. This suggest that there is an interaction occurring between a discrete state of DCE that couples to a background continuum process. This Fano resonance does not appear to be present in an argon matrix isolation.

Acknowledgements

Throughout this process I have been supported and encouraged by my supervisor Dr John Harrison, who showed great perseverance and patience during this rather more drawn out process than intended. Without his inspiration and excitement for this field of study this thesis would not exist.

Special thanks to Dr Marie-Anne Thelen for the support, advice and assistance provided. To Dr Debbie Jordan for moral support and a laugh when needed.

Thanks to my mother, Margaret McNie, for kicking me when I said I was bored and starting me on this path and rest of my family for supporting me in more ways than I can mention.

Contents

Figures

Tables

Introduction

The aim of this thesis is to investigate the supercritical properties of argon and its effect and ability as a solvent for trans-1,2-dichloroethylene (DCE). This is to be measured in a specially designed and constructed cells using ultraviolet-visible and infrared spectroscopy.

Supercritical fluids are achieved when a substance is at or above its critical temperature and critical pressure. This can be seen in the Figure 1 below. In the supercritical region the properties of both the liquid state and gas state are combined giving a lower density and viscosity which in turn should lead to an increased solubility of solid and gas substances, fast diffusion of solute, faster mass transit and therefore an increase in the reaction rate (Engel & Reid, 2006). A supercritical fluid allows for a range of properties depending on where the conditions of pressure and temperature are in relation to the critical point of the chosen substance. Closer to the critical temperature and an increase of density is seen, increasing pressure also effects the density, by being able to adjust the conditions it allows for increased solubility across a range of compounds.

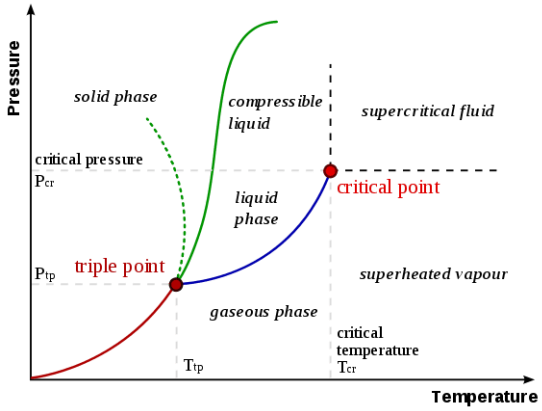

Figure 1: Image of critical point and phase boundaries sourced from https://www.thoughtco.com/definition-of-critical-point-605853

Supercritical fluids are already used for a range of applications both in research and industry, supercritical carbon dioxide extraction of caffeine from coffee beans is the classic example. It is the tuneable ability of supercritical fluids as solvents that makes them highly functional, they are used in extraction, polymer, pharmaceuticals and many other applications (Ke, et al., 2009). The ability of a compound to be soluble in a supercritical gas can be adjusted using the vapour pressure, temperature and pressure; generally, a higher vapour pressure leads to a higher solubility (Darr & Poliakoff, 1999). Supercritical xenon has a relatively high polarizability of 4.01×10^{-24} cm^3 this allows it to be a good solvent for organic solids compared to other noble gases (McHugh & Seckner, 1984). Using a supercritical rare gas system is useful as it allows the macroscopic density function effects to be singled out for the analysis (Nishikawa, 20007).

Supercritical fluids have been shown in the use of chemical reactions to enhance a preferred pathway to produce specific products. In organic solvents hydrogen has low solubility; this is shown by the reaction of $Fe(CO)_4$ with H_2 in n-heptane where the $Fe(CO)_4$(heptane) is dominant. Using the unique properties of supercritical fluids, you can dope a molecule into a reaction that otherwise would be very difficult. Seeding H_2 into supercritical argon allows for the formation of $Fe(CO)_4(H)_2$ as the dominant product, this is just one use (Besora, et al., 2009). Supercritical argon has also been used as a solvent in the extraction of components such as hydrocarbons from soil samples; it is inert and relatively inexpensive along with a suitable window in the infrared region for online analysis (Liang & Tilotta, 1998). Both krypton and xenon are good supercritical rare gas solvents they have been used in many cases but they are considerably more

expensive than and therefore not as practical as argon (Calladine, Vuong, Sun, & George, 2009).

For this experiment argon was chosen as it is a relatively cheap and easily accessible compared to other noble gases and has an achievable supercritical point. argon has a critical temperature of 150.687 K and critical pressure of 47.994 Atm (Shimanouchi, 1972). The supercritical relationship can be clearly seen in Figure 2 below where holding the pressure constant at 50 atmospheres a distinct phase boundary point is visible between supercritical and liquid phases. If the temperature is reduced below 150 K a liquid state is present. Also seen is a significant drop in density in the supercritical region if the temperature increases above 152 K, this gives a small temperature target window where solubility should be the most successful.

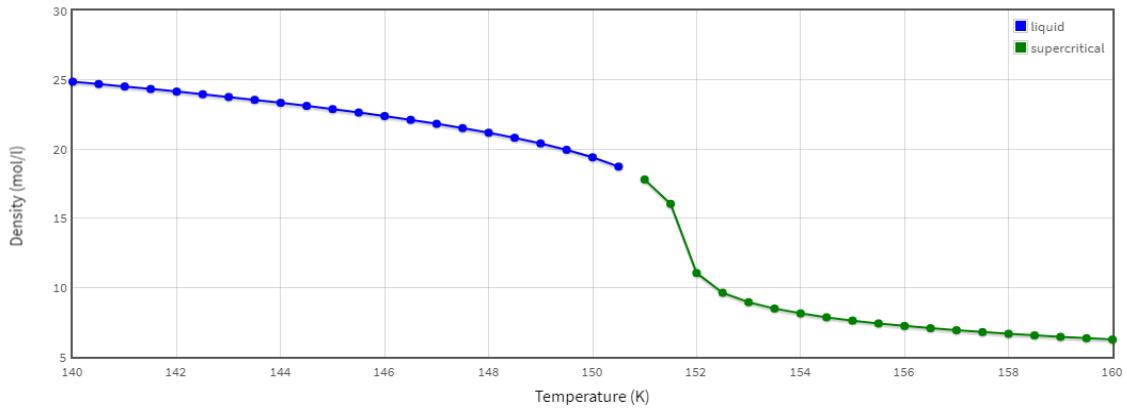

Figure 2: Graph of density change of argon 140 K to 160 K at constant pressure of 50 atm https://webbook.nist.gov/cgi/fluid.cgi? (Shimanouchi, 1972)

When looking at the phase diagram from constant 151 K temperature and changing the pressure (Figure 3) there is the expected phase change from vapour to supercritical and the density increase as pressure increases. However, this

also shows that the range where the sharpest density rise is broader from 48 atmospheres to 50 atmospheres. This allows for more fluctuation in the pressure of an environment, while retaining the increased density to enhance solubility than a temperature change will allow.

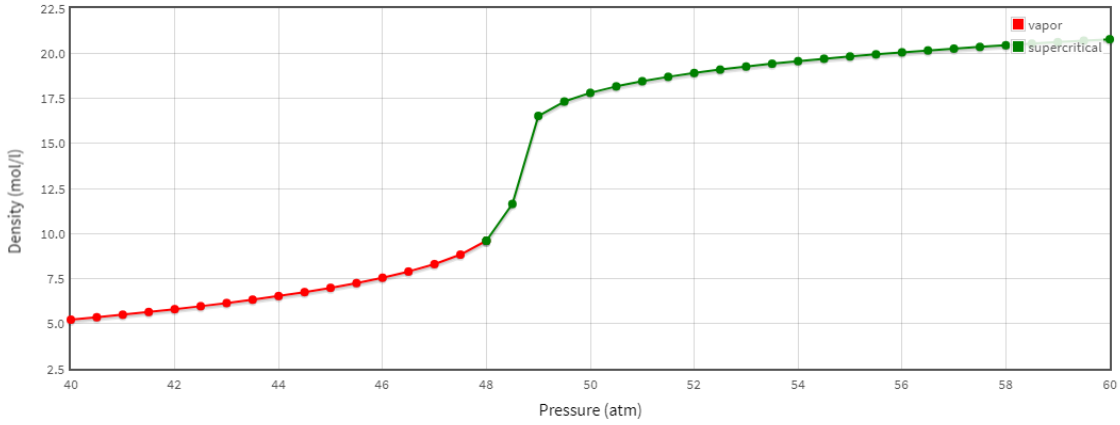

Figure 3: Graph of density change of argon at various pressures from 40 atm to 60 atm at constant temperature of 151 K https://webbook.nist.gov/cgi/fluid.cgi? (Shimanouchi, 1972)

Using the supercritical point conditions for argon as a design reference a sealed static cell was constructed. This required an internal sample cell which can be temperature controlled and withstand up to 55 atmospheres of pressure. It needed to be encased in an external vacuum casing to create a high vacuum for a helium cryo-cooler to operate under. It required windows on both the internal and external casing that could be aligned, and finally it all needed to fit into the ultraviolet-visible spectrophotometer and fourier transform infrared instruments.

Trans-1,2-dichloroethylene (DCE) (Figure 4) was selected as a test sample for investigation in supercritical argon for a number of reasons. It is a small, volatile, well studied molecule (Craig, 1998) that has distinctive infrared peaks (Table 1) and shows high intensity in the ultra-violet region at low concentrations.

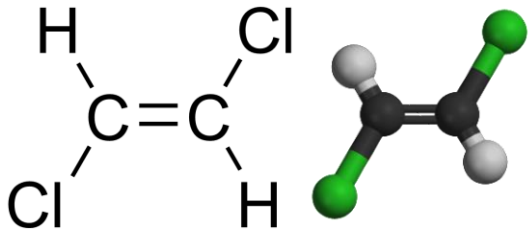

Figure 4: Skeletal and ball and stick representation of trans-1,2-dichloroethylene (DCE)

Infrared symmetry C_{2h} vibrations for DCE	
a_u CH bend (v_6)	899.8 cm^{-1}
b_u CH stretch (v_9)	3090 cm^{-1}
b_u CH bend (v_{10})	1200 cm^{-1}
b_u CCl stretch (v_{11})	828 cm^{-1}

Table 1: IR energies levels taken from https://webbook.nist.gov/cgi/cbook.cgi?ID=C156605&Mask=800#Refs, (Shimanouchi, 1972)

The advantage of a volatile sample in testing allowed for gas phase analysis in the static cell set up before any argon was added. This also ensured enough sample was present without needing to heat the cell or design in a way to physically mix the DCE with the argon.

The over-reaching end goal of this process is to is to take the solubility knowledge gained and construct a molecular beam pulsed valve in which supercritical argon is seeded with trans-1,2-dichloroethylene (DCE). A supersonic molecular beam

is obtained through the adiabatic expansion of a gas from a high pressure container into a high vacuum, the internal energy of the beam and therefore the internal temperature drops as the energy is converted into translational energy (Harrison). When the internal temperature and the mean velocity associated with random thermal motion drops, there is also a decrease in rotational and vibrational energy. Seeded noble gas beams which contain a low percentage (typically around 1-5%) of the selected molecules can be used to achieve low rotational temperatures as the beam acts as a heat sink (Demtroder, 1996) The advantage of the supersonic molecular beam is that it isolates the molecule from solvent interactions and along with the cooling gives a simplified spectroscopy result. This gives a larger amount of information about the structure and dynamics of the molecule than is available through a typical condensed phase method.

Supercritical solvents are preferred over liquid solvents in molecular beams as liquids inevitably freeze at the source blocking the small opening when they are being expanded into the vacuum. It is then essential to assess the solubility information gathered and determine how well supercritical argon has interacted with the DCE before the pulsed molecular beam source is developed. This is particularly difficult design process as it needs a dynamic seal that does not leak under high vacuum conditions as it is required to be pulsed. The high pressure and low temperature will also add interesting challenges in the development of the source. A system for the injection of the non-volatile molecules into the supercritical argon source will need to be developed. This pulsed source will be able to be analysed using a mass spectrometer. If supercritical argon can be used in this way it would open a pathway to generation of slower moving beams (due

to the lower internal energy of the argon, almost all of which is transformed into kinetic energy in the adiabatic expansion process). There is also the possibility of carrying out reaction chemistry at low temperatures for detection of novel species and new reaction pathways by using a static cell.

Initial Cell Design

The main components of the cell are crafted from copper, aluminium, quartz, stainless steel Swagelok fittings, Teflon and indium foil. The cell is crafted from a short piece of copper rod, 51 mm long and a diameter of 31 mm, with the sample window cut right the way through. On the copper block a gasket of 0.5 mm of indium foil (Sigma Aldrich 357286-9.24) was placed followed by the 2 mm thick quartz glass window (GM Associates cut from JA0003). A 0.5 mm thick piece of Teflon sheet was placed between the window and aluminium bracing block which helps smooth out any rough areas in the surrounding metal and prevents the

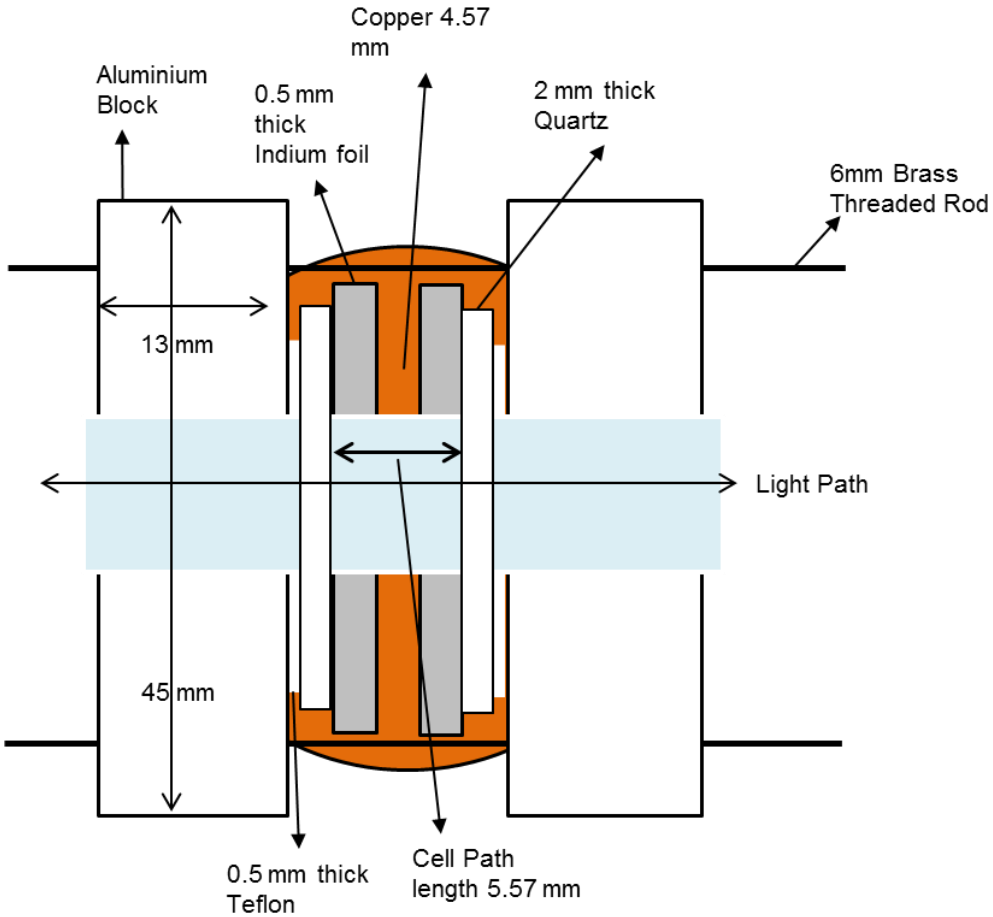

Figure 5: Cross-section diagram of initial cell design

window from cracking when the window is compressed onto the cell. The quartz windows are braced to withstand the 50 atmosphere pressure by aluminium blocks, which are secured through the copper with four 6 mm threaded brass rods; these were capped with stainless steel nuts and spring washers.

The copper cell is attached via two aluminium spacer blocks to a longer length of copper rod (diameter 31 mm and length 150mm) which is connected to a Varian Cryo-Compressor Model 313-0010. The two rectangular aluminium blocks allow the cell windows to be aligned correctly while still maintaining the heat transfer required for cooling. The first block is 65 mm long by 35 mm high and 18 mm thick with the second block being 65 mm long by 35 mm high and 10 mm thick. One stainless steel $^1/_8$" NPT to $^1/_8$" Swagelok elbow at the top of the cell attaches to the gas or vacuum line as required, along with a straight stainless steel Swagelok $^1/_8$" NPT to ¼" Swagelok screw fitting with removable ¼" Swagelok cap

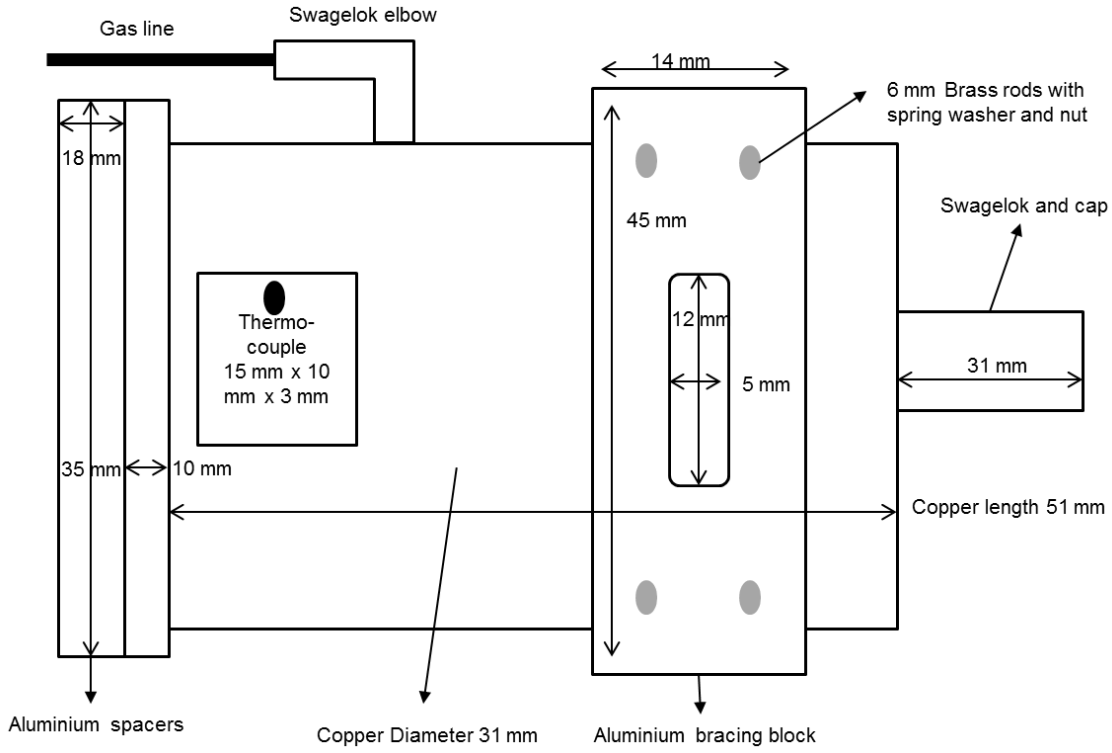

Figure 6: Initial cell diagram profile

at the end that allows the sample to be introduced into the window cavity. A thermal sensor from Lake Shore, DT-471 silicon diode sensor, is attached to the copper block of the cell allowing for constant monitoring using a Lake Shore 211 Temperature Monitor of the cell temperature and the first aluminium spacing block has two resistors attached which provides the ability to control the cell temperature to within ± 1 Kelvin while the scan was running and also for warming the cell up. The current for the resistors was controlled by a Hewlett Packard E3630A Triple Output DC Power Supply, manually controlled.

The cell is enclosed in an outer vacuum chamber comprised of two stainless steel rings which are 105 mm in outer diameter by 15 mm thick, giving an inner diameter of 75 mm, overall length is 52 mm. The two rings were sealed with Viton O-rings and braced together with an aluminium plate at each end.

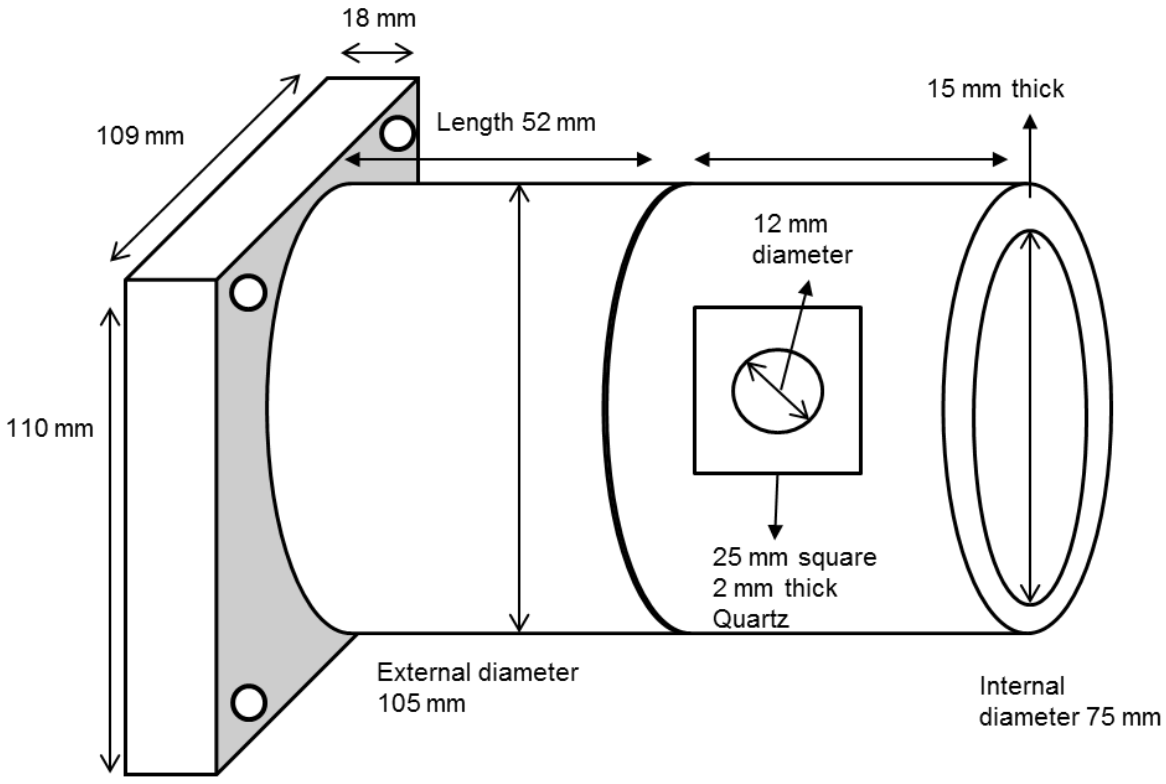

Figure 7: Diagram of external vacuum casing dimensions

These plates were 110 mm high by 109 mm long and 18 mm thick. There are four 10 mm stainless steel threaded rods secured through the corners of each aluminium block clamping the structure together and the vacuum was provided by an Edwards RV5 rotary mechanical pump.

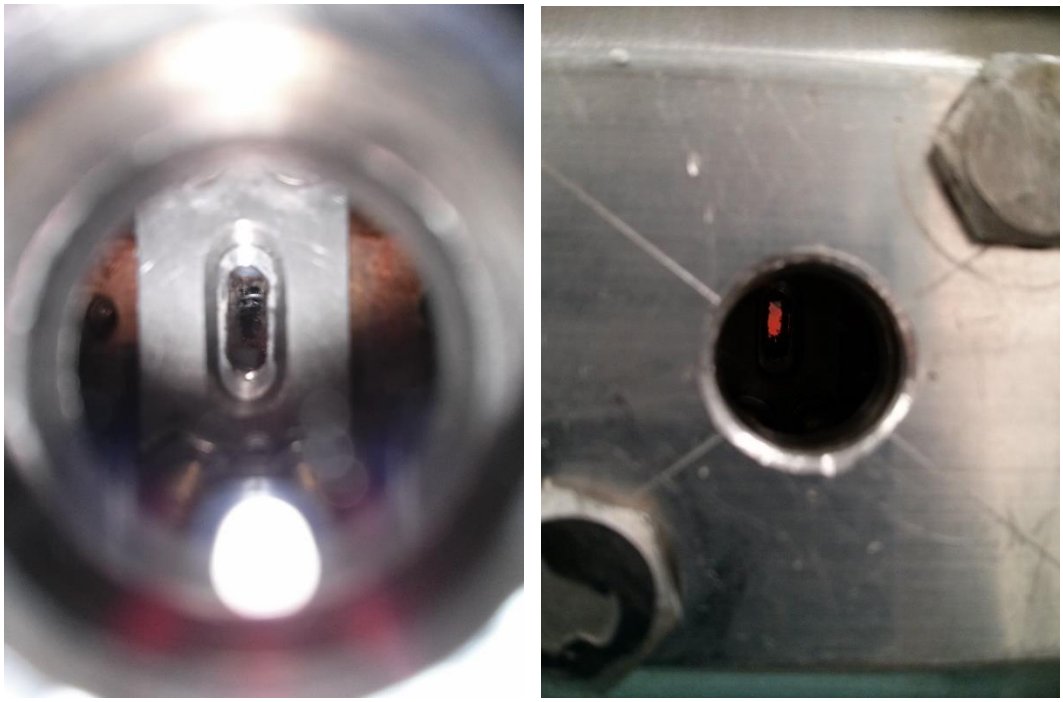

Figure 8: Photo of initial internal cell through external casing window and photo of external window aluminium bracing plate looking through external and internal windows

Due to the need to pass visible or ultra-violet light through the sample in the inner cell, a path for the light had to be constructed in the outer casing as well. The second ring has two 12 mm diameter holes opposite that provide this window through which the light can pass, to maintain the vacuum outer windows consists of 25 mm long by 25 mm high and 2 mm thick quartz squares that are sealed with a Viton O-ring and held in place with either a 2 mm thick aluminium brace or sellotape.

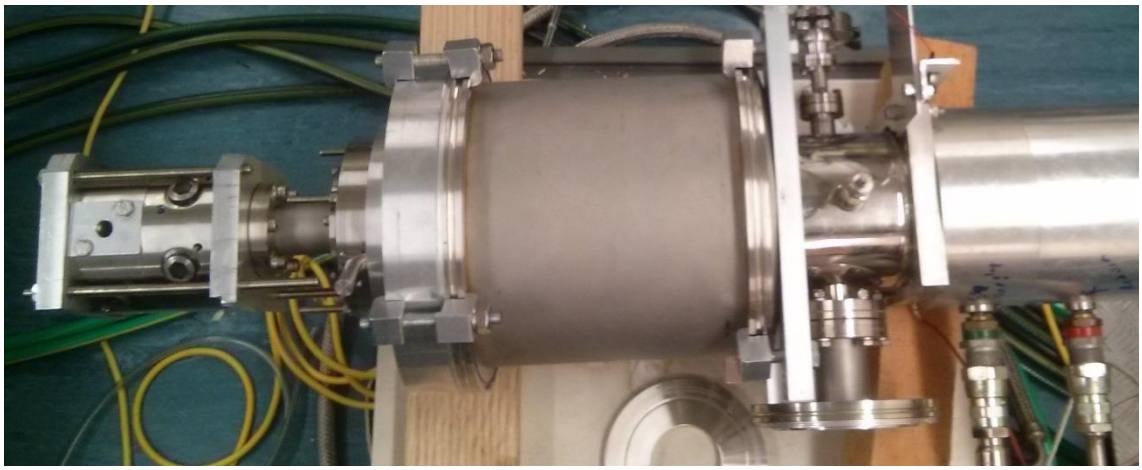

Figure 9: Photo showing external vacuum casing attached to cryo-cooler

The entire outer cell structure fits into the sample compartment of the UV-2700 Shimadzu spectrophotometer, the first aluminium block fits tightly into the opening of the spectrophotometer and blocks off the entrance to stop any external light passing through to the detector. This is further reduced by covering the join with aluminium foil and then in black fabric, the fluorescent lights in the room were also turned off when scans were running.

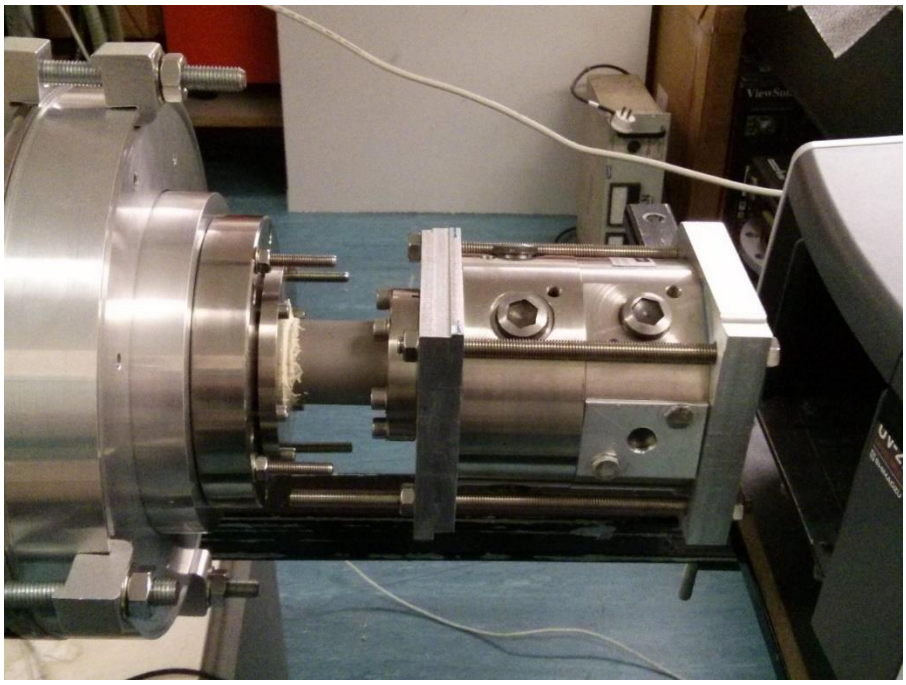

Figure 10: Photo of initial cell lined up with UV-Vis spectrophotometer

This combination of metals allows for a good transfer of the cooling capacity from the cryo-compressor and will withstand the temperature and pressure requirements that supercritical argon needs. However, there are some issues with the current design, the indium foil cold flows and will eventually creep into the window and block the light. The bracing blocks need to be tightened after every couple of cooling and warming cycles to prevent leaks forming around the windows, it is a fine balancing act as tightening the blocks too much will push more indium into the cavity and the non-perfect surfaces results in unbalanced pressure and the breaking of the quartz windows. There is currently no easy way to remove the flowed indium with the windows still attached and removal of the windows without breaking them is near impossible.

The main issue encountered during construction revolved around sealing the cell at the windows and at the sample port. Initial designs of the sample port were to try a bolt with a modified end that would screw into the copper and seal around a 1 mm thick Teflon disk. The Teflon worked well at room temperature with the 50 atmosphere pressure but as the cell was cooled down it would leak and additional tightening did not help. The Teflon would flow and get stuck in the groves which presented an additional problem as you could not easily get the Teflon seal out. This sample port was upgraded to a screw in stainless steel Swagelok with cap fitting that sealed with no troubles and the cap is easily removed allowing a sample product to be introduced into the cell cavity.

The other main area of development was securing the quartz windows both on the inner cell and also on the outer vacuum casing. For the outer ring there was an added challenge with the restriction in space in the spectrophotometer sample chamber, none of the windows or seals could be too thick. The outer ring casing had two 12 mm diameter holes already cut so development was only required to find a way to seal the outer quartz windows for the vacuum. This involved machining an O-ring grove, placing the 25 mm by 2 mm thick quartz square on the O-ring, protecting with a 0.5 mm thick square of Teflon, and bracing it with a 2 mm thick rectangle of aluminium which was screwed in at two corners. This worked surprising well after a few teething problems, however when one of the windows broke, we found that placing the quartz window onto the O-ring and holding it in place at the corners with pieces of sellotape worked just as well and did not leak noticeably when drawing the vacuum.

The inner quartz windows provided more of a challenge; most combinations could withstand the high pressure at room temperature but as the cell was cooled, they would eventually leak. To add more complexity as the cell warmed up, they tended to reseal which made leak checking particularly difficult, solid carbon dioxide was used to cool the cell without requiring the outer vacuum casing which enabled leak testing at colder temperatures. Initial design consisted of two pieces of 0.5 mm Teflon sheet place either side of the quartz window, this arrangement withstood the 50 atmosphere pressure at room temperature but as the cell was cooled it started to leak, tightening of the supporting blocks did yield some success at cooler temperatures but could only really achieve one cooling cycle before cell started to leak, more tightening resulted in the quartz cracking.

The second attempt was to use a silicone sealant to affix the quartz onto the copper block. This showed initial promise but it also had the same issues of leaking as the cell was cooled, the silicone was somewhat interesting as not only did it not retain a seal at cooler temperatures it hardened due to the cold and this actually managed to crack one of the windows. The final option was indium foil, there was some hesitation regarding its use due to the toxicity and handling concerns around it, however it proved to be the most robust way to seal the windows and is able to be cycled a couple of times before a leak develops and the aluminium bracing blocks need to be tightened.

Design of Molecular Beam Valve

The molecular beam valve is a lab built system that involves a copper cylinder attached to the closed cycle helium refrigerator. The copper cylinder is the backbone of the valve and has a cavity in the centre which houses the Teflon encased magnet; the magnet is made of neodymium, with Teflon spaces and a standard ball point pen spring to supply tension. The face plate of the valve is made from aluminium and has a 0.25mm hole drilled in the centre. There is a 2 mm thick Teflon seal between the aluminium and copper and the face plate is sealed with 6 screws. Copper wire was coiled around the main copper body, insulated by a 1mm Teflon sheet.

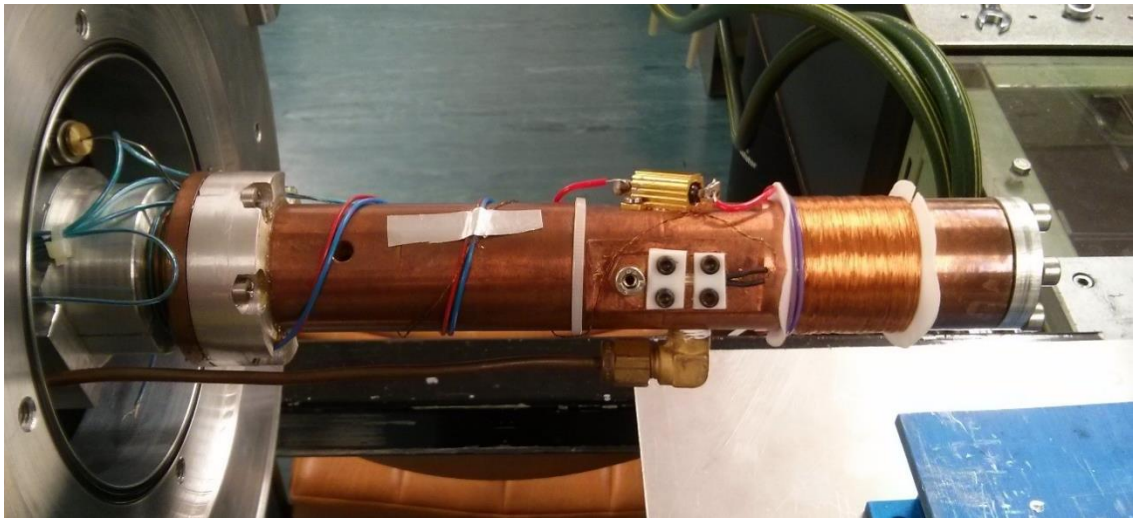

Figure 11: Photo of molecular beam pulsed valve

The reservoir section is an aluminium vessel that provides a cavity through which the argon must pass. It involves a stainless steel tube that extends into the bottom of the reservoir with the next connection following through to the valve higher on the side causing the argon to flow down through the sample and then back out to the valve. The reservoir is also heat sunk to the cooler using an aluminium block to help with the cooling rate. Both the reservoir and the valve have a thermocouple to measure the individual temperature at either end; there was generally a 1.5 to 3 kelvin difference with the reservoir being the colder. There are also resisters to provide heating, each pair of resistors are controlled separately, however there was only one Lake Shore 211 Temperature Monitor making control more difficult.

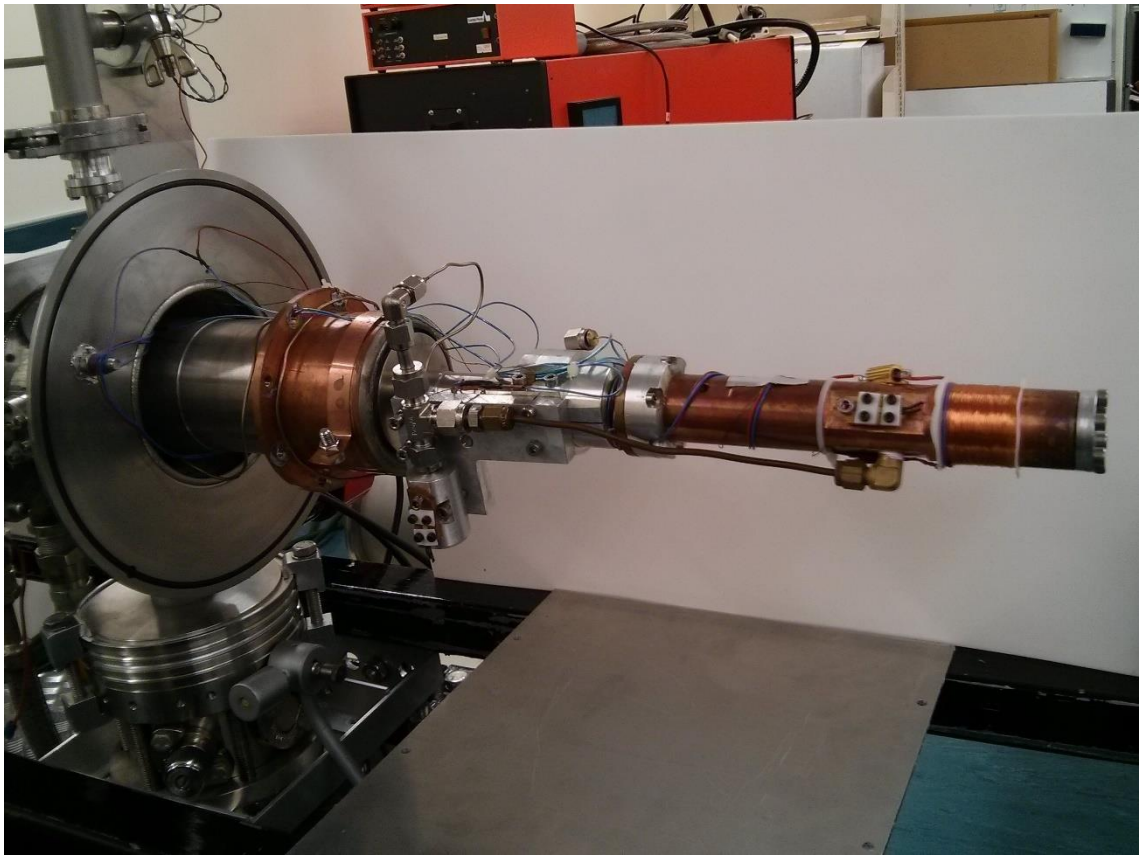

Figure 12: Photo of full pulse valve including sample reservoir

This valve feeds in to an arrangement of differentially pumped chambers called a source chamber, main chamber and an ultra-high vacuum chamber. The valve is in the centre of the main vacuum chamber, the beam passes through a skimmer and any additional gas is directed to the source chamber through an extension of the source chamber into the main. The main chamber is pumped by an Edwards Diffstak model 100LN2 diffusion pump which is roughed out by an Edwards RV5 roughing pump.

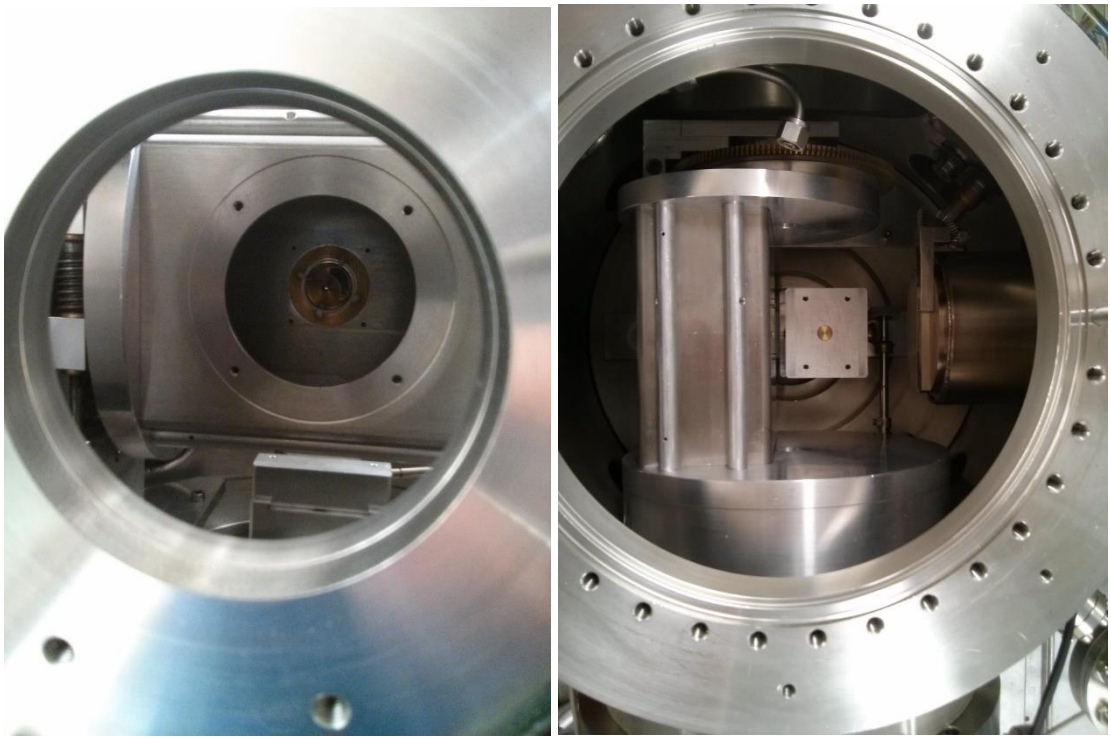

Figure 13: Left photo of source chamber and skimmer from perspective of valve entry direction. Right photo of source chamber from above with top removed

The source chamber has a larger capacity with a CIT-ALCATEL crystal 160E diffusion pump and Edwards E2M18 roughing pump. The valve is aligned on the same axis with the mass spectrometer with a small gate valve in between the ultra-high vacuum chamber connected to the mass spectrophotometer. The ultra-

high vacuum is created by two turbo pumps, main turbo is an Edwards Ext 250M controlled by an Edwards EXC 300M control unit. The second smaller turbo is a LH turbovac 50 turbomolecular pump, controlled by a LH turbotronik NT50 control unit.

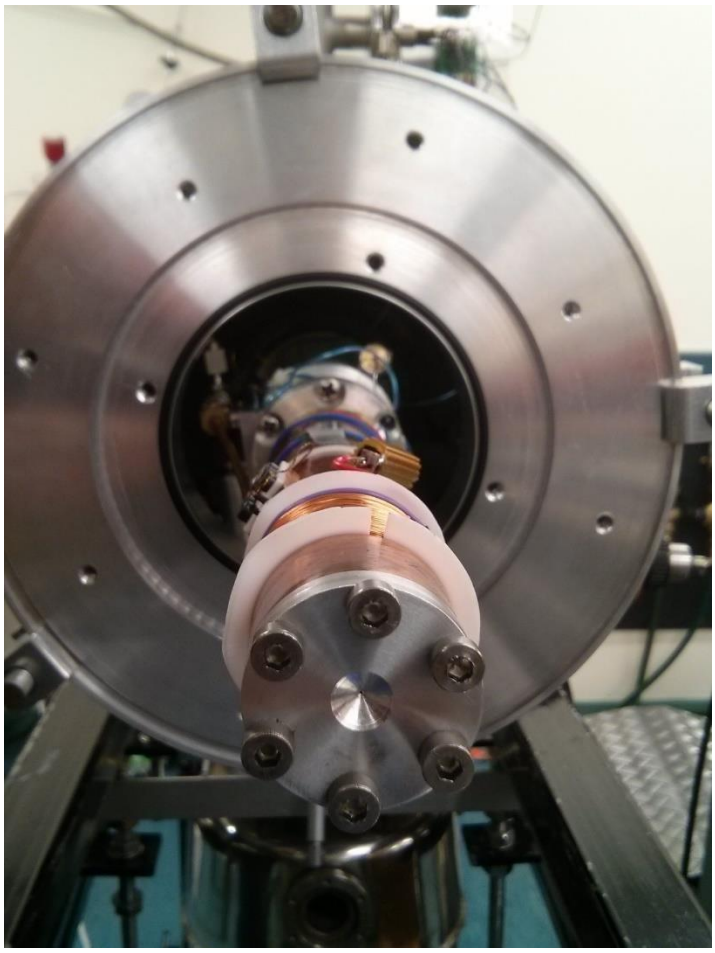

Figure 14: Photo of valve face plate

Some of the design issues encountered in the molecular beam construction are typical of working with cold temperatures, the valve will work perfectly at room temperature but as the valve cools it stops sealing. This was the main problem in this case and took a large amount of runs and trials to get a system that might function for only one cooling cycle. Initial design included a magnet on a movable

stage that would be moved closer to the valve magnet to use the repulsion forces to help move the internal magnet; this was removed with the main issue being unable to align it correctly and it proved to not be needed. It was replaced with a fine skimmer that proved to be too small and was upgraded to a larger skimmer that worked well. The face plate initially had a 1.0 mm hole which proved to be difficult to get the Teflon coated magnet to securely seal against when the valve was pulsing, the hole was reduced to the 0.25 mm which showed marked improvement.

Infrared Cell Design

Due to the limitations of the initial cell structure a second more robust design was created which allowed for the analysis in a Nicolet iS50R FT-IR. This cell took the principles of the first cell design and improved upon them. The cell consists of a copper block (7.5mm x 6.8mm x 4.5mm) with three windows, two parallel for IR and UV analysis and a third window at the front to allow for fluorescence analysis. The parallel windows are 25mm diameter by 6mm thick barium fluoride held in place by a copper bracing block and six hex stainless steel screws with spring washers. Again, indium foil is used as a gasket between the main copper cell and the windows and Teflon spacers used to pack between the window and the window retaining rings. With a circular window bracing block design for the retaining rings giving an easier controlled window bracing pressure along with an improved indium cutting there is a reduction in the indium cold flow issues seen in the first dell design. The issues with windows needing to be tightened during each run still remain and this continues to be a balance between sealing against the 50 atmosphere pressure required and breaking the windows. The front window is also 25 mm diameter and 6 mm thick made of quartz.

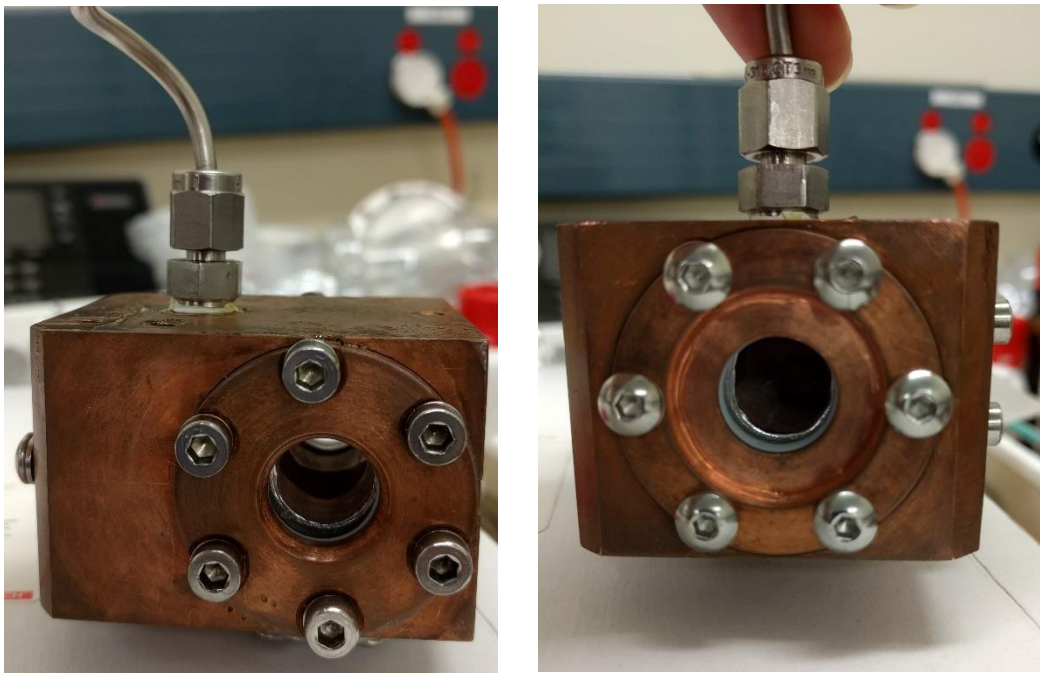

Figure 15: Left photo of side view of IR cell. Right photo a front view of IR cell showing third window to allow for fluorescence

The copper cell block is attached to the copper rod of the cryo-cooler CH204N coldhead attached to a HC-4E1 compressor (Sumitomo Heavy Industries Inc.) using three stainless steel hex screws, a layer of Apiezon-N vacuum grease is used between the two pieces of copper to provide good thermal conductivity. The cell is connected to the gas lines using 1/8” stainless steel Swagelok tubing and 1/8” male NPT to Swagelok adaptor. The temperature is controlled using a Lake Shore 325 temperature controller and a heating rod (2W) is embedded centrally in the copper heat transfer rod. The temperature is monitored using a thermal sensor from Lake Shore, DT-670-BO silicon diode sensor attached to the top front corner of the cell. High pressure situations in the cell is monitored with a 3000 psi MKS baratron (750C33PCE2GA) and MKS PDR2000 Dual Capacitance Manometer readout. For low pressure situations a 1000 torr MKS baratron (622A13TBE) was used with a multifunctional Ion gauge controller Model ICG100 by Stanford Research Systems.

Figure 16: Photo of top view of cell showing 3 connection points to connect to cryo-cooler

This entire cell is enclosed in an aluminium vacuum casing with 8 external window options. For this analysis the external barium fluoride 25mm diameter by 2 mm windows were aligned. This casing is attached to the main cooler vacuum system via a NW160 O-ring that allows the casing to be rotated while under vacuum. The external vacuum is created by an Edwards RV5 backing oil pump and an Oerlikon Leybold vacuum turbo drive TD400 turbo pump controlled by a Leybold turbo control 300. The backing pressure was monitored using an Edward's PRM10 pirani gauge and Edwards Controller 1101 long with an Ion gauge controlled by a Leybold-Heraeus IONVAC IM 210.

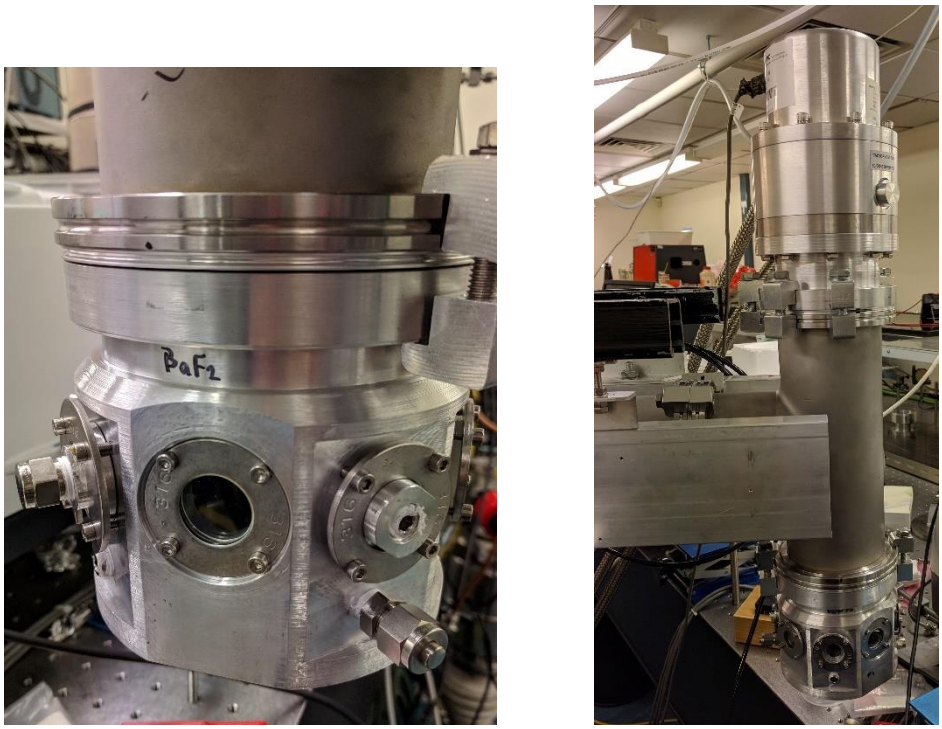

Figure 17: Left photo of external vacuum casing showing external window. Right photo of cryo-cooler set-up attached to external window casing

This cell arrangement is connected to a rolling frame that allows the cell to be pushed into the Nicolet iS50R FT-IR for analysis or pulled out and twisted to the side to access the unit away from the instruments. This functionality is required as the matrix stage is designed to swap out for the infrared cell and use the same external vacuum casing. The Thermo-Fisher Nicolet iS50R FT-IR is equipped with a liquid nitrogen cooled mercury cadmium telluride detector which was used for this work. The wavelength range at the lower energy end of the spectrum was limited by the BaF_2 optics of the cell and vacuum housing to around 800cm^{-1}. The upper end of the spectrum is detector limited at around 7000 cm^{-1}.

Matrix Stage Design

The matrix set up is interchangeable with the infrared cell in the vacuum chamber. The matrix stage consists of a 25mm BaF_2 window mounted using indium foil for thermal contact on a copper block which is cooled down using a CH204N coldhead attached to a HC-4E1 compressor (Sumitomo Heavy Industries Inc.) and the temperature monitored and controlled with a Lakeshore 325 temperature controller and Lakeshore, DT-670-BO silicon diode sensor. The stage allows for a thin layer of solid argon deposited using a low flow ¼" Swagelok metering valve. The trans-1,2-dichloroethylene is deposited by passing 1-2 atmospheres of argon through the sample container taking trans-1,2-dichloroethylene vapour and depositing it in a solid argon matrix. The stage is then aligned in the Nicolet iS50R FT-IR

Methods

Method of Initial Cell design in Ultraviolet-Visible Spectrophotometer

0.05mL of trans-1,2-dichloroethylene (Sigma Aldrich, D62209) was pipetted into the cell using an HTL 0.02 mL to 0.2 mL auto pipette, with 1 atmosphere of room temperature argon (BOC) flowing through the system. Cell was sealed with argon still flowing and the vacuum casing assembled around the inner cell. Cell and sample were cooled overnight using a helium Cryo-Compressor (Varian Cryo-Compressor 311-0010) to obtain working temperature. The sample was aligned in a UV-2700 Shimadzu ultraviolet visible spectrophotometer. Using the UVProbe Ver2.42 software the sample was scanned from 260nm-190nm on the very slow scanning mode, with a slit width of 0.1nm, sampling interval of 0.05, and accumulation time of 0.5 seconds. Each temperature and pressure combination were scanned a minimum of three times

Determination of initial cell volume.

An enclosed metal cylinder with valve was attached to the pipe work taking argon to the cell and the entire unit was vacuumed out using an Edwards E2M2 mechanical Pump. The pressure was monitored using a 3000 psi MKS baratron (750C33PCE2GA) and MKS PDR2000 Dual Capacitance Manometer readout. 31 atmospheres of argon gas at room temperature was added to the cylinder only and stock argon cylinder was sealed off, valves throughout the line were opened and the corresponding pressure drop was recorded. Volume of the metal cylinder was determined by weighing the empty, under vacuum, cylinder. The cylinder was then filled with distilled water, density 0.9966g/ml, and the change in mass was used to determine the volume.

Molecular Beam Sample Addition Method

1 mL of trans-1, 2-dichloroethylene (Sigma Aldrich, D62209) was introduced into the reservoir using a syringe, with 1 atmosphere of room temperature argon (zero grade, BOC) flowing through the system. The reservoir was sealed with argon still flowing and the valve unit was sealed into the vacuum chamber. Valve and sample were cooled overnight using a helium cryo-compressor (Varian Cryo-Compressor 311-0010) to obtain working temperature. The valve was pulsed at various temperatures and pressures with the beam passed through a skimmer. Beam was then fed into a RGA300 mass spectrophotometer with a filament current from 1.0 to 2.5 (mA) and electron multiplier from 2000V to 2350V.

Method for Infrared Cell

Trans-1,2-dichloroethylene (DCE, Sigma Aldrich, D62209) vapour was introduced into the cell using the gas line system. 5 mL sample of DCE was placed into a sample reservoir which was cooled down using liquid nitrogen and the system was pumped to remove any contaminates. The sample vessel was then warmed up using a heat gun. This freeze-pump-thaw cycle was repeated 3 times. The cell and lines were pumped out to less than 1 torr monitored using a 1000 torr MKS baratron (622A13TBE) and ion gauge controller model ICG100 readout by Stanford Research Systems. The sample vessel was then opened and the vapour pressure of trans-1,2-dichloroethylene filled the system. The pressure across the lines and into the cell was measured at 243 torr. The cell was then cooled down to 210 K before the argon (zero grade, BOC) was added to the system and the pressure was increased slowly up to 51 atmospheres.

Temperature was monitored and controlled with a Lakeview 325 temperature controller and Lakeshore DT-670 silicon diode sensor. The sample was aligned in a UV-2700 Shimadzu ultraviolet visible spectrophotometer. Using the UVProbe Ver2.42 software the sample was scanned from 260 nm - 190 nm on the medium scanning mode, with a slit width of 2 nm, sampling interval of 0.2 nm, and accumulation time of 0.5 seconds. The cell was then aligned in the Nicolet iS50R FT-IR and 32 scans at 0.125 cm^{-1} wavenumber interval were undertaken using OMNIC software.

Method for Matrix Stage

The matrix stage was cooled down to 20 K. The cell was aligned in the Nicolet iS50R FT-IR and 32 or 64 scans (for the background) at 0.125 cm^{-1} wavenumber interval were taken using OMNIC software. Using a low flow ¼" Swagelok metering valve a thin layer of solid argon (zero grade, BOC) was deposited upon the window over a period of around 20 minutes to obtain a background. The trans-1,2-dichloroethylene (Sigma Aldrich, D62209) vapour is then introduced to the stage in 1 atmosphere of argon through the DCE reservoir. Deposition continued for sufficient time to obtain high signal/noise spectra.

Results and Discussion

Initial Ultraviolet-Visible Spectroscopy Cell

The initial cell construction focused on the ultraviolet-visible spectrum and absorbance change as conditions were varied to assess the link between the solubility of trans-1,2-dichloroethylene to the temperature and pressure conditions of argon.

The scans were obtained at various pressures (atmosphere, Atm) and temperatures (kelvin, K) covering the gas, liquid and supercritical states of argon. Temperatures of 140 K, 150 K, 160 K, 170 K, 190 K, and 210 K, along with pressures of 1 Atm, 20 Atm, 40 Atm, 50 Atm, and 55 Atm, were combined to achieve the required conditions. Each set of conditions were scanned three times, due to alignment issues encountered the baseline for each individual scan was subtracted before the three scans were averaged.

A trend was seen across the three lower pressure conditions of 1, 20 and 40 atmospheres. As the temperature was decreased at the lower pressures in which argon was still in its gas phase the absorbance of trans-1,2-dichloroethylene was visibly reduced. This is seen when comparing the 210 K and 190 K scans, the absorbance of trans-1,2-dichloroethylene decreases significantly across these two temperatures. With a normal melting point of 223.27 K, trans-1,2-dichloroethylene still shows significant absorbance at 210 K, 23 K below its freezing point, in 1 atmosphere of argon. The absorbance increases at this

temperature as the argon pressure is increased, despite still being in its gas phase the density increase is enough to improve solubility.

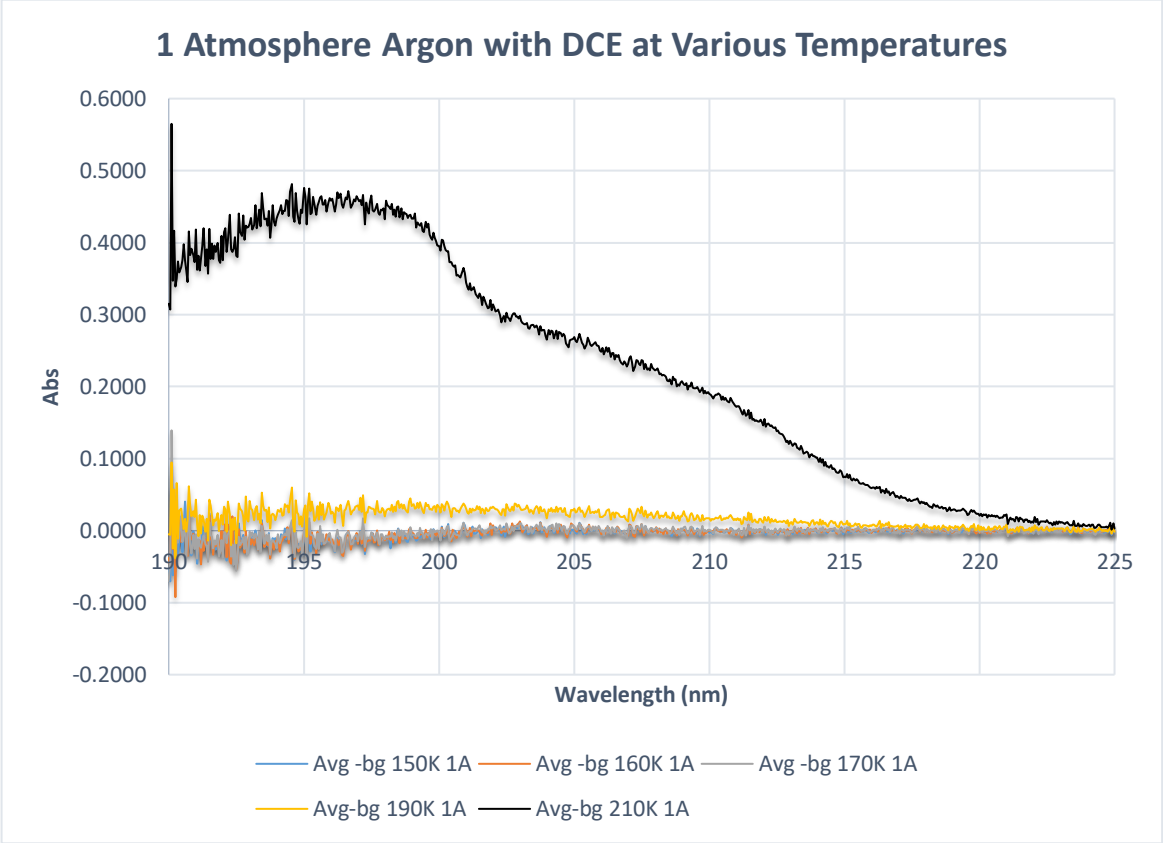

Figure 18: Changing absorbance of DCE with temperature at a constant 1 atm of argon

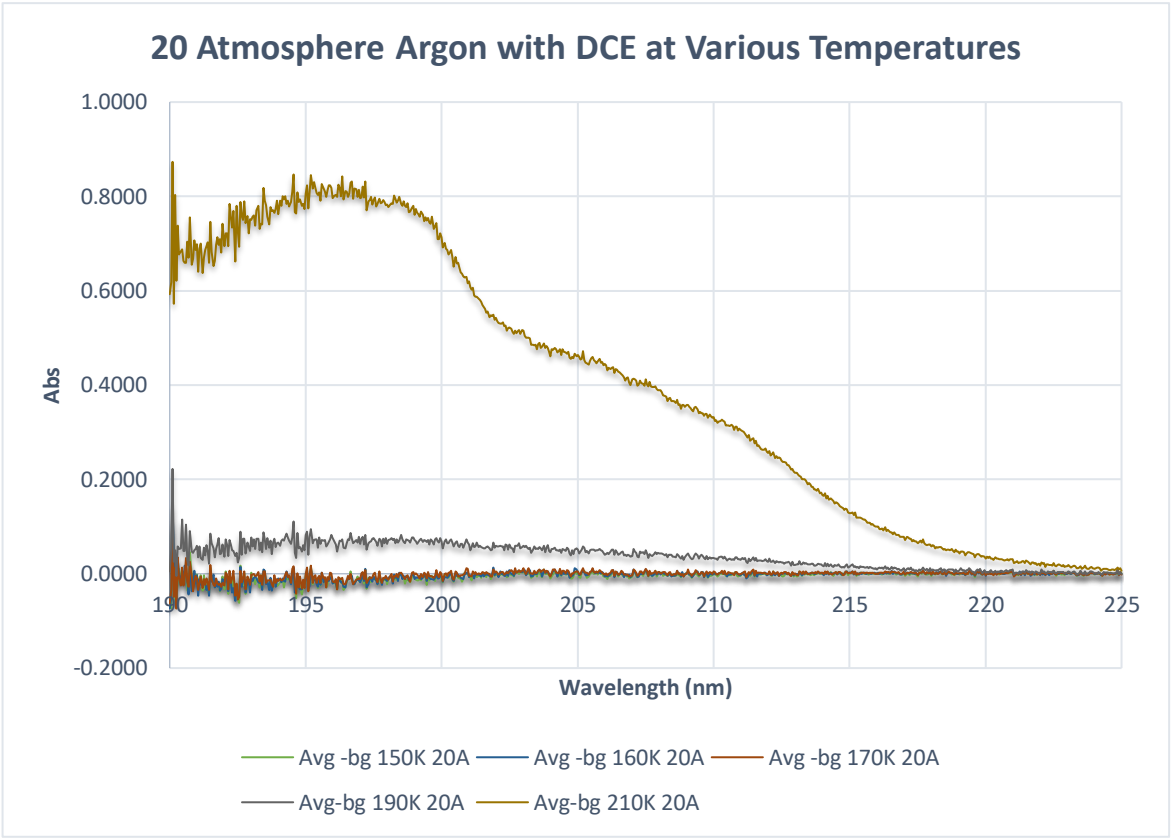

Figure 19: Changing absorbance of DCE with temperature at a constant 20 atm of argon

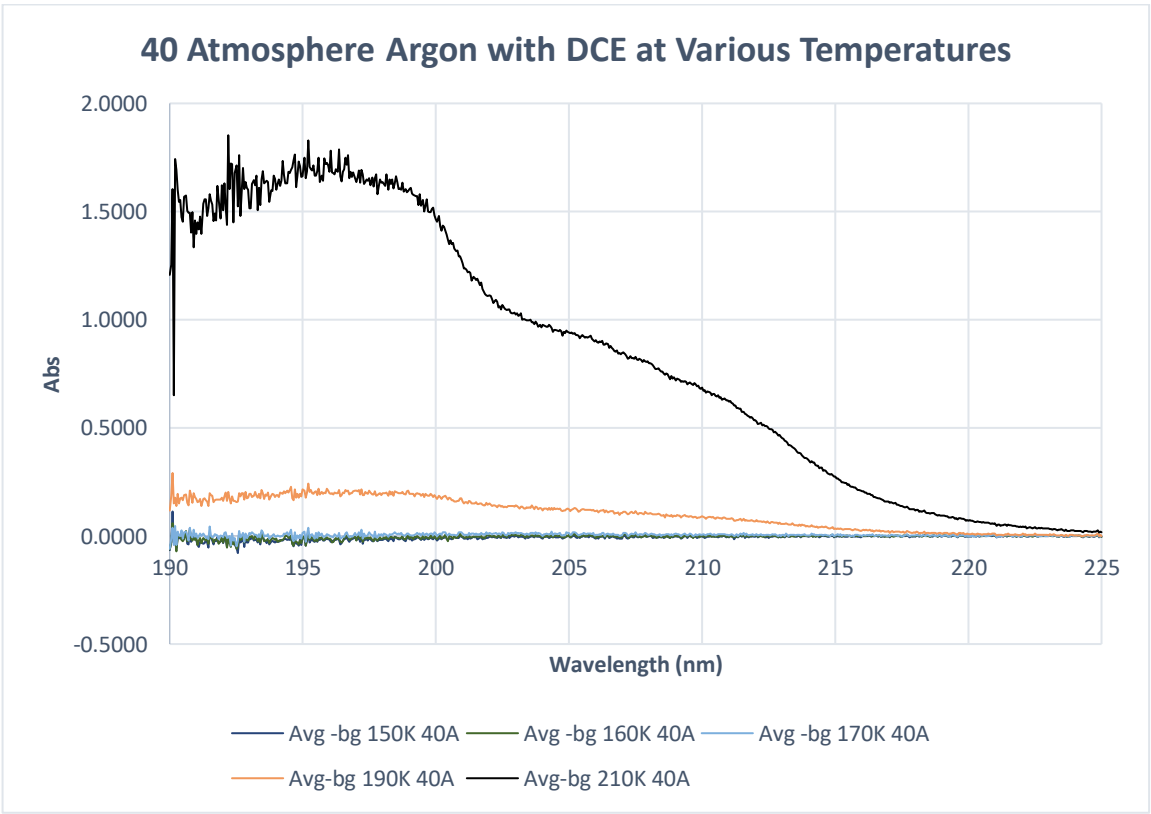

Figure 20: Changing absorbance of DCE with temperature at a constant 40 atm of argon

When the temperatures and pressures in the cell were aligned to give either liquid or supercritical argon the absorbance increased dramatically despite the reduction in temperature. This is seen in the scans at 50 atmospheres (Figure 21) most noticeably. When the conditions were pushed into the liquid argon region of 140 K at 50 atmosphere a strong absorbance was also observed.

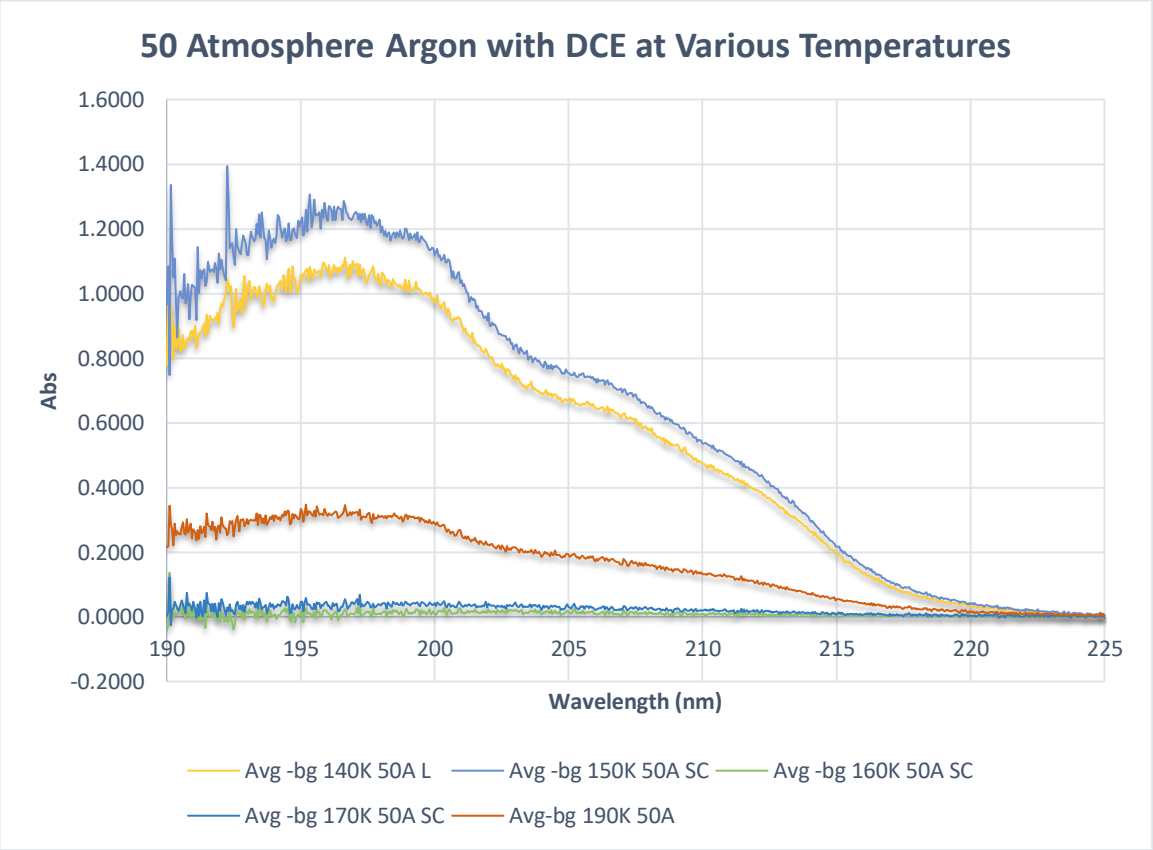

Figure 21: Changing absorbance of DCE with temperature at a constant 50 atm of argon

However, when the supercritical region is reached (see the scans below at 55 atmospheres, Figure 22) the closer you get to the supercritical point temperature of 151 K the stronger the absorbance becomes. This can be seen clearly by comparing the absorbance of the 150 K scan verses the 160 K scan. Despite the

conditions technically being in the supercritical region it is only when the temperature is within a couple degrees of the supercritical point that the relationship between the density increase and the increased solubility of trans-1,2-dichloroethylene occurs.

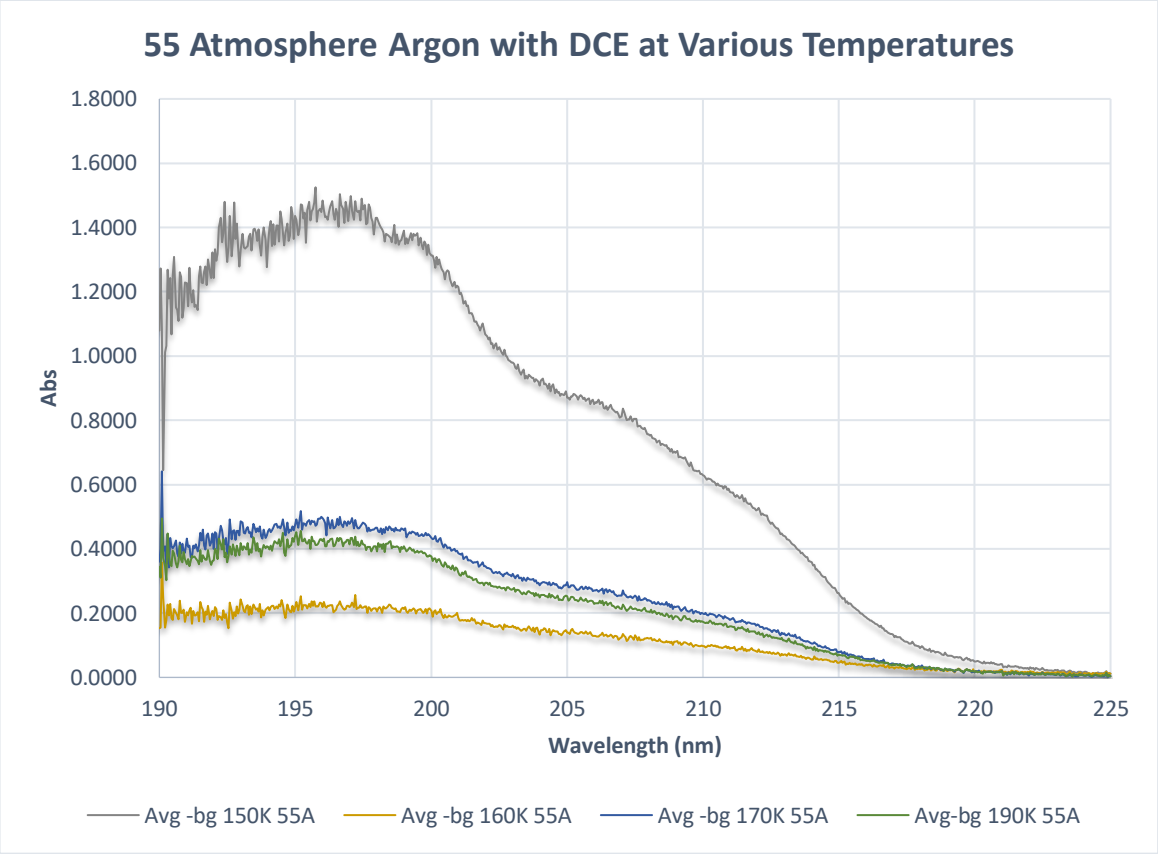

Figure 22: Changing absorbance of DCE with temperature at a constant 55 atm of argon

One issue encountered during analysis is the trans-1,2-dichloroethylene photolysing, due to the presence of the UV light, the absorbance peaks of 190.15 nm and 192.20 nm related to the chloro-acetylene by product increases (Guckert, 1990). The concentration of the DCE vapour in the cell was calculated using the molar absorptivity value of 21077.0 ± 1204.4 L mol^{-1} cm^{-1} at 193 nm obtained from the cross section of 3.5 ± 0.2 $x10^{-17}$ cm^2 listed on the MPI-Mainz UV/Vis Spectral Atlas of Gaseous Molecules of Atmospheric Interest website (Keller-Rudek, 2013) and the path length of the cell at 0.65 cm. As this wavelength is close to

the chloro-acetylene peaks the concentration found at 193 nm was used on the same scan to obtain the molar absorptivity for trans-1,2-dichloroethylene at 205nm outside the interference of the acetylene. The volume of the cell was determined to be 2.983 cm^3 which allowed the concentration to be converted into moles and using the density of argon at different pressures the mole fraction of trans-1,2-dichloroethylene was determined.

The calculated mole fraction used the moles of trans-1,2-dichloroethylene at 205 nm for each temperature and pressure is shown on the table below, (Table 2).

Temperature and pressure	DCE mole fraction		Temperature and pressure	DCE mole fraction
150K 1A	0		140K 50A	3.16E-06
160K 1A	5.71E-06		150K 50A	4.64E-06
170K 1A	7.15E-06		160K 50A	2.74E-07
190K 1A	4.87E-05		170K 50A	7.25E-07
210K 1A	5.32E-04		190K 50A	5.75E-06
150K 20A	0		150K 55A	4.82E-06
160K 20A	2.15E-07		160K 55A	1.76E-06
170K 20A	1.86E-07		170K 55A	5.03E-06
190K 20A	4.13E-06		190K 55A	5.92E-06
210K 20A	4.45E-05			
150K 40A	0			
160K 40A	0			
170K 40A	3.39E-07			
190K 40A	4.83E-06			
210K 40A	4.31E-05			

Table 2: DCE mole fractions at various temperatures and pressures

These mole fractions show an exponential reduction in the amount of trans-1,2-dichloroethylene at 1, 20, and 40 atmospheres as the temperature drops (Figure 23, Figure 24, Figure 25). At 50 Atm (Figure 26) the 190 K, 170 K and 160 K show the exponential reduction similar to the lower pressures with a clear spike in mole fraction at the 150 K. There is not a clear relationship at 55 atm scans which are all at supercritical conditions, however they do show an increase at 150 K compared to 160 K, confirming that these seem to be more dependent on how close to the 150.687 K supercritical temperature point the scan was taken at (Figure 26). The supercritical scans also show an improved absorbance at 190 K consistent with the lower pressure scans at the same temperature

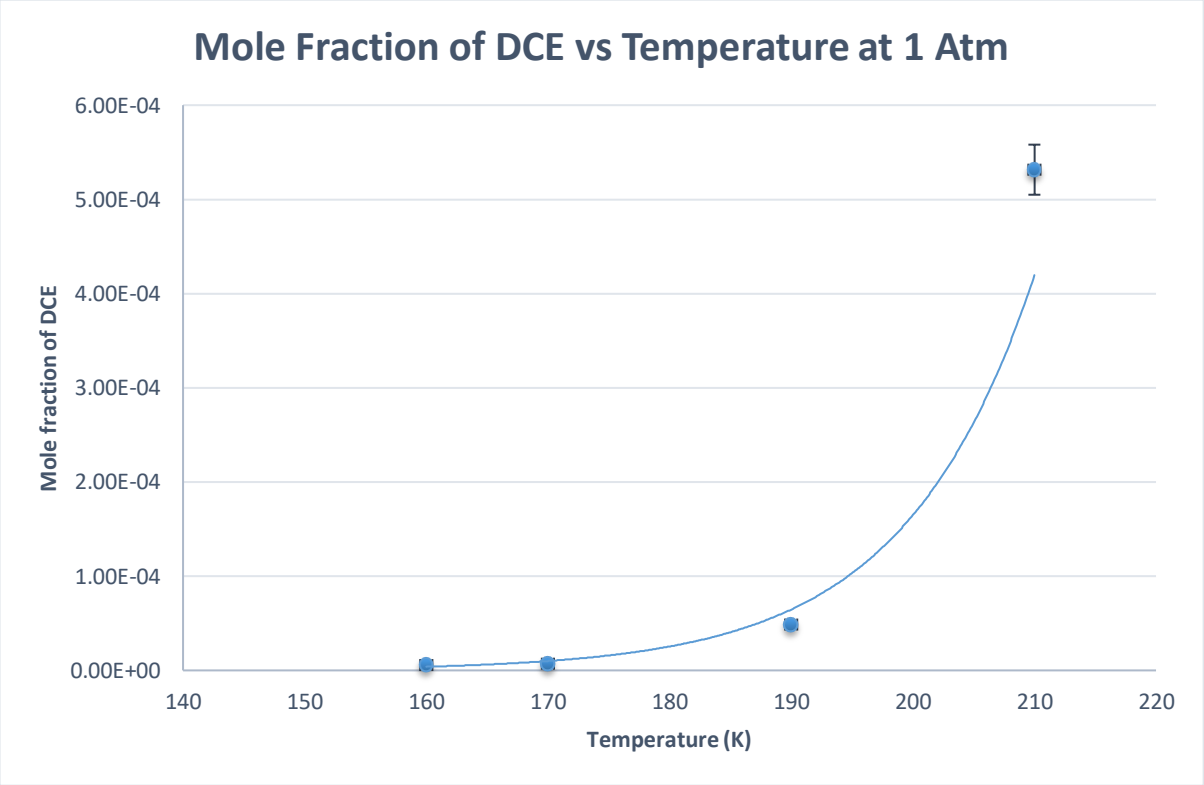

Figure 23: Mole fraction of DCE relationship with 1 Atm of argon at various temperatures, equation of line $y = 1E\text{-}12e^{0.0935x}$, $R^2 = 0.9707$

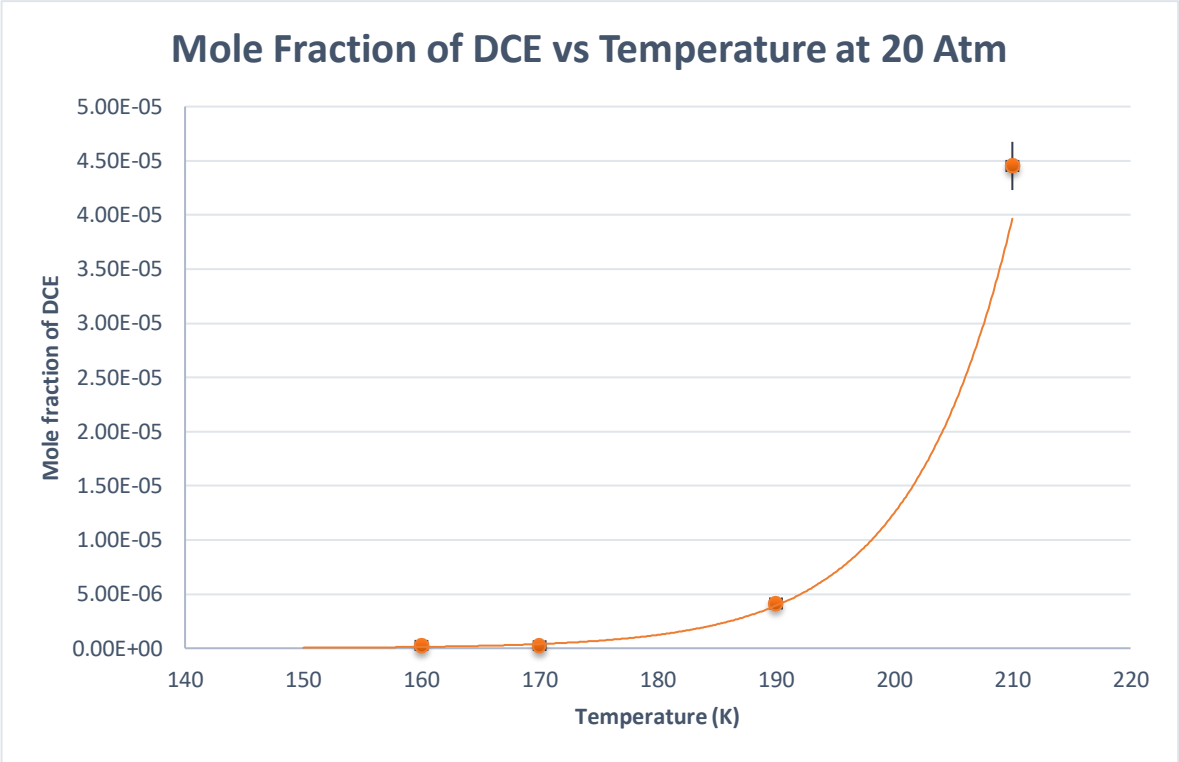

Figure 24: Mole fraction of DCE relationship with 20 Atm of argon at various temperatures, equation of line $y = 1E\text{-}15e^{0.1156x}$, $R^2 = 0.9575$

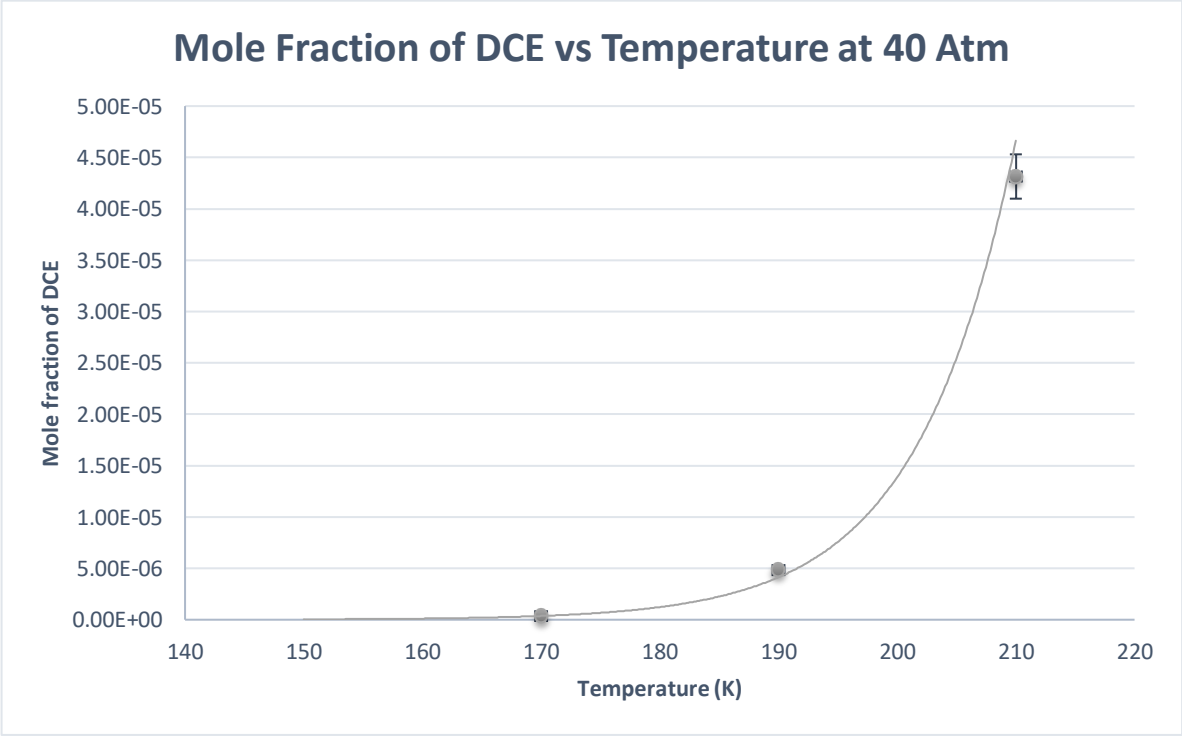

Figure 25: Mole fraction of DCE relationship with 40 Atm of argon at various temperatures, equation of line $y = 4E\text{-}16e^{0.1211x}$, $R^2 = 0.9969$

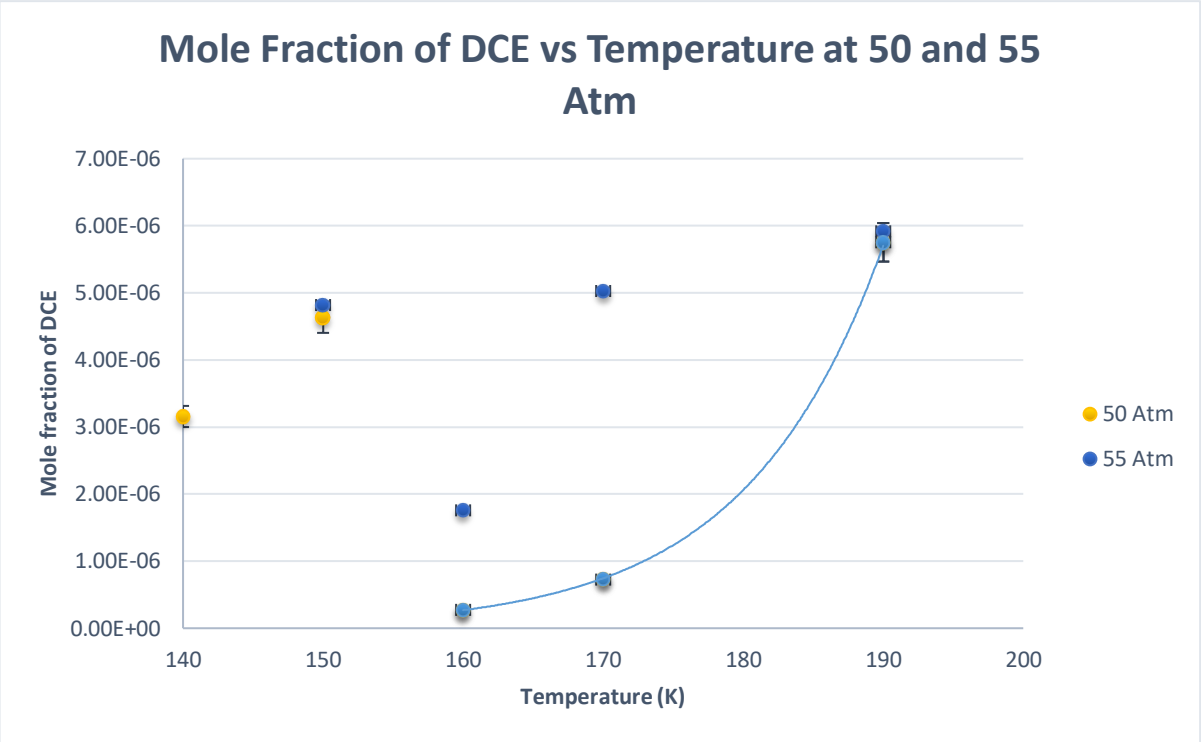

Figure 26: Mole fraction of DCE relationship with 50 and 55 Atm of argon at various temperatures, equation of line $y = 2E\text{-}14e^{0.1018x}$, $R^2 = 0.9998$

There is a clear trend between the pressure and temperature when the argon is in a gaseous state. As the pressure increases, and therefore the density, the intensity of trans-1,2-dichloroethylene also increases. This enables argon to act as a solvent for trans-1,2-dichloroethylene and becomes significantly more efficient at the supercritical point. Limitations in the cell design and temperature control equipment restricted the ability to do fine temperature changes around the supercritical point of argon. However, there were enough promising results from the initial ultraviolet-visible spectroscopy analysis to indicate that the supercritical state of argon will work as solvent for trans-1,2-dichloroethylene in a molecular beam set up. As explained in the cell construction section this was designed and attempted to run however, many manufacturing and equipment limitations resulted in no viable results. Attention was redirected to the second cell design that allowed for infrared spectroscopy analysis.

Molecular Beam Pulsed Valve

Despite getting some design improvements during this process it proved extremely difficult to align the valve, not leak around the faceplate or magnet and have enough trans-1,2-dichloroethylene dissolved in the supercritical argon flowing past to get results in the mass spectrophotometer. A large limitation was the cryo-cooler that was not cooling efficiently and had what appeared to be a 1 to 3 K temperature difference between the reservoir potentially causing the trans-1,2-dichloroethylene to freeze in the sample reservoir. As seen in the ultraviolet-visible scans the best solubility environment was right at the supercritical point of argon with the inability to control the temperature with a level of stability across the whole pulsed valve there was not a consistent flow of supercritical argon through the whole system.

Infrared Cell

Ultraviolet-Visible Spectroscopy

The infrared cell design was initially tested in the ultraviolet-visible spectrophotometer to ensure that there was a consistent response of trans-1,2-dichloroethylene with supercritical argon to the initial cell results. This was complicated due to a small leak around the windows that restricted the ability to hold the cell at high pressure leading to a reduction in pressure over time. Further addition of argon proved sufficient to keep the pressure constant and there was sufficient DCE in the cell in the condensed phase that allowed equilibrium to be maintained. The cell was initially cooled to 150 K with 27 to 30 atmospheres of argon present to minimise the backing pressure increase and turbo pump failure. With the improvements in design, such as a vapour sample and path length increase in the cell an immediate increase in intensity of trans-1,2-dichloroethylene was seen. The cooling pattern was repeated and a clear reduction in intensity was observed as the temperature fell below 190 K at 30 atmospheres pressure. When supercritical conditions of 151 K and 49.2 atmospheres were reached the intensity increased as seen before and showed a significantly increased intensity comparable to the 190 K at 29.5 atmosphere conditions.

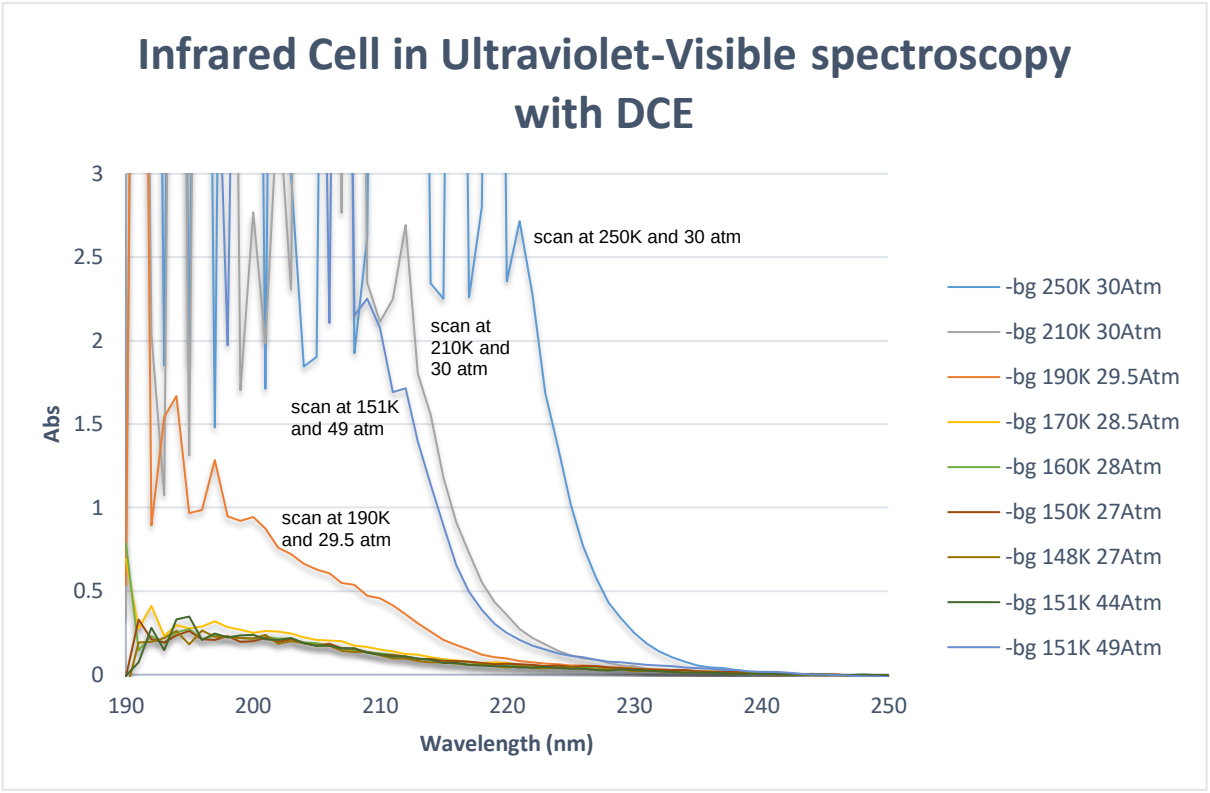

Figure 27: UV-Vis spectrum of DCE at various temperatures to test infrared cell.

Infrared spectroscopy

To assist in managing the pressure leaking from the cell at low temperatures the trans-1,2-dichloroethylene sample was added into the cell and a reduced 30 atmospheres of argon was added to flush the trans-1,2-dichloroethylene out of the line. The cell was then cooled down to 140 K with scans taken at various intervals, this allowed the argon to freeze in the hole and stop the leak, which sealed the cell before 50 atmospheres of argon was added. The infrared scans showed transition through multiple states of the trans-1,2-dichloroethylene during this process. Although the iS50R was purged with nitrogen it was found that it was not possible to reduce the water background sufficiently to eliminate interferences in the strongest absorbing regions. However, there is little spectral overlap between the background gas absorptions and the DCE absorptions so that this was not limiting. All spectra were collected at the highest obtainable resolution of 0.125 cm^{-1} with 64 scans being accumulated for the background and typically 32 for the sample spectra.

As can be seen from the sample spectra below this was sufficient to give high signal to noise in the regions of interest (Figure 34). The background was collected with the cell empty and at room temperature. This had the disadvantage that spectra at the lowest temperatures suffered from a baseline drift particularly evident around the lowest energy region (800-900 cm^{-1}) coinciding with slight changes in absorbance of the window materials near their spectral cut off. The system was also susceptible to small changes in the alignment of the cell giving

an additional baseline drift. This is inevitable due to the contraction with temperature of the copper used in construction of both the coldhead and the cryo-cell. As long as proper care was taken not to bump the mobile stand the apparatus was mounted on such changes were minimal when compared to the strength of the absorption of the DCE. To avoid any vibration from the cold head being transmitted to the FTIR during the experiment the FTIR was independently mounted on a 3 x 1.5 m optical table (Newport RS2000) completely vibrationally decoupling the two parts.

There are four strong or very strong infrared transitions of interest for trans-1,2-dichloroethylene, they are b_u CH stretch (v_9), b_u CH bend (v_{10}), a_u CH bend (v_6) and b_u CCl stretch (v_{11}) given in Figure 28. These appeared consistently in the scans, however as expected the peak shapes changed as the conditions changed.

Vibrational and/or electronic energy levels

Go To: Top, References, Notes

Data compiled by: T. Shimanouchi

Symmetry: C_{2h} Symmetry Number σ = 2

Sym. Species	No	Approximate type of mode	Selected Freq. Value	Rating	Infrared Value	Phase	Raman Value	Phase	Comments
ag	1	CH str	3073	C	ia		3073	S p liq.	
ag	2	CC str	1578	C	ia		1578	S p liq.	
ag	3	CH bend	1274	C	ia		1274	S p liq.	
ag	4	CCl str	846	C	ia		846	S p liq.	
ag	5	CCCl deform	350	C	ia		350	S p liq.	
au	6	CH bend	900	B	899.8	VS gas	ia		
au	7	Torsion	227	C	227	M gas	ia		
bg	8	CH bend	763	B	ia		763	M dp liq.	
bu	9	CH str	3090	C	3090	S gas	ia		
bu	10	CH bend	1200	B	1200	S gas	ia		
bu	11	CCl str	828	B	828	VS gas	ia		
bu	12	CCCl deform	250	D	250	W gas	ia		

Figure 28: IR energy levels taken from https://webbook.nist.gov/cgi/cbook.cgi?ID=C156605&Mask=800#Refs (Shimanouchi, 1972)

Initial scans of pure trans-1,2-dichloroethylene (DCE) vapour at 298 K (Figure 33, Figure 34, Figure 35) resulted in intense peaks indicative of the b_u CH stretch (ν_9) and of the b_u CH bend (ν_{10}) in the gas phase, the CH bend (ν_6) and b_u CCl stretch (ν_{11}) are strongly absorbing and showed intense rotation data for DCE in its vapour state. The (ν_9) and (ν_{10}) peaks showed the most change in shape and position as conditions changed, these peak wavenumbers have been summarised in Table 3. An initial test of the cell involved trans-1,2-dichloroethylene (DCE) vapour being cooled down from 298 K to 150 K under 1 atmosphere argon, these scans at various temperatures showed a reduction in absorbance, consistent with the ultra-violet visible scans previously undertaken, this can be seen clearly from the three absorptions at b_u CH stretch (ν_9), b_u CH

bend (v_{10}) and a_u CH bend (v_6) (Figure 30, Figure 31, and Figure 32). There is also a visible baseline between the 298 K scan and the next at 250 K, this shift due to the cooling of the cell creating changes in the window alignment which is most noticeable between these two temperatures.

As expected, there was loss of rotational detail, though no position shift, as the pressure of argon was increased to 30 atmospheres due to pressure broadening of the peaks, however there was still plenty of detail to continue. The very strong peaks at (v_{11}) and (v_6) were intense as expected and generally off scale (Figure 35) they showed the expected change in being pressure broadened but were too intense to show the same level of shape or position change. The (v_9) and (v_{10}) peaks showed clear broadening with loss of detail, most clearly seen with the disappearance of the central peak at (v_9) (Figure 33: IR scan of DCE vapour compared to high pressure broadened peak at Figure 33).

During the running of the cell with trans-1,2-dichloroethylene (DCE) in 50 atmospheres of argon, DCE was in various states as conditions changed leading to a range of peak shapes and positions. At 212 K with 36 Atm of argon a significant peak shift at (v_9) of 5 cm^{-1} compared to the broadened gas phase indicates that liquid DCE is present, this is confirmed by the reduction in the 3101 cm^{-1} gas peaking creating a shoulder (Figure 36). The liquid state shape difference is again seen at the (v_{10}) where the peak has moved 2 cm^{-1} and formed a shoulder (Figure 37). This comparison between the gas phase spectra strongly suggests a liquid layer of DCE has formed on the windows giving rise to the peak

shifts. The presence of shoulders shows that there is still DCE vapour present in the cell interacting with the argon and not all the DCE is in a liquid state.

When the cell reached 140 K and the argon pressure was increased to 49 Atm resulting in liquid argon conditions a peak shape changed which was different from liquid DCE seen previously. The (v_9) shows two quite sharp peaks, the weaker aligns with the gas phase peak showing that some DCE vapour is still present. The stronger absorbance peak has shifted another 7 cm^{-1} and narrowed considerably from the liquid DCE peak. This suggest that there is both solid and gas DCE present. When comparing this to a supercritical scan at 151 K with 50 atm of argon, the (v_9) spectrum is very similar pattern is seen, however there is a reduction in the gas peak showing that less gas DCE is present in the supercritical environment along with a sharpening of the solid peak. Both liquid argon and supercritical argon environments showed a baseline asymmetric lineshape leading up to the (v_9) and (v_{10}) peaks. This lineshape is deviates downwards more sharply for the supercritical scan (Figure 38).

For the (v_{10}) peak (Figure 39) there is still a baseline asymmetric lineshape deviation on a lesser scale to the (v_9) however the two scans replicate the same pattern where the liquid argon scan shows a more intense middle peak which appears to be associated with the DCE gas phase which is reduced in the supercritical argon environment comparatively compared to the liquid environment, though there is still a substantial shoulder present to some degree.

This baseline deviation did not have a clear cause. The cell was held at 151 K and the argon was pumped out, this allowed for a scan of the sample that had frozen solid on the windows of the cell. This showed a (v_9) peak associated with the solid DCE that continued to show (Figure 40) the same baseline deviation with some of the residual peaks associated to the gas state of DCE removed, this showed that there was a thin layer deposition of solid DCE on the windows. For (v_{10}) two intense peaks, one with a shoulder, are seen indicating solid DCE is present. There is also a strong correlation between these peaks and the calculated anharmonic infrared frequencies calculated for each isotope combination using Gaussian 09 see Table 4. The presence of Fermi resonance has also allowed for these peaks isotope contributions to be better resolved.

The (v_9) and (v_{10}) peaks were compared between the supercritical argon and the residual solid environments. This showed that there was no significant improvement in resolution of the peaks, however there is clearly some dissolved DCE in the supercritical environment along with some baseline peaks associated with the argon. Despite improved resolution in the solid phase for DCE, specifically compared to the condensed phase, these peaks are not as sharp and resolved as a solid DCE state run in an argon matrix, which is also 31 cm^{-1} shifted off the peaks seen in the supercritical environment or evacuated cell.

Infrared symmetry C_{2h} vibrations for trans-1,2-dichloroethylene (DCE)							
a_u CH bend (v_6) cm^{-1}	b_u CH stretch (v_9) cm^{-1}			b_u CH bend (v_{10}) cm^{-1}			b_u CCl stretch (v_{11}) cm^{-1}
NIST							
900	3090			1200			828
Gas Phase	Gas Phase			Gas Phase			Gas Phase
281K, 1 Atm, gas phase DCE with no argon present							
off scale	3101.338	3095.680	3019.980	1206.062	1200.406	1196.163	off scale
	Gas Phase			Gas Phase			
281K, 1 Atm, gas phase DCE with argon high pressure							
off scale	3101.338		3092.007	1205.759		1196.466	off scale
	Gas Phase			Gas Phase			
212K, 36 Atm, Liquid DCE forming layer on windows in argon							
broad 896.700	3101.338		3086.724	1204.485 S		1198.716	broad 822
	Gas		Liquid	Gas		Liquid	

140K, 49 Atm, DCE in Liquid argon										
			3094.902	3079.876	3076.202 S	1203.679	1199.593	1196.897	825.849	broad 822.
			Gas	Solid		Solid	Gas	Solid		
151K, 49 Atm, DCE in supercritical argon										
905.332	898.760	826.331	3095.726	3079.294	3076.020 S	1203.423	1200.707	1196.964		broad 826
			Gas	Solid		Solid	Gas	Solid		
155K, no argon, Solid DCE layer on windows										
905.389	898.359			3078.662		1203.276	1201.709 S	1196.890		
				Solid		Solid		Solid		
8K, Matrix, DCE deposited with argon										
			3110.643	3106.589	3104.337	1202.294	1201.872	1200.492		
20K, Matrix, DCE deposited with argon										
			3110.206	3106.428	3104.125	1202.133	1201.658	1200.131		

Table 3: Summary of observed peaks of DCE in various states and conditions

Calculations of trans-1,2-dichloroethylene Cl Isotopes

Anharmonic calculations using Gaussian 09 (M. J. Frisch, 2017), at the rmp2(frozen core)/cc-pVqz level of theory were used to give a better picture of the anharmonic infrared energies and Fermi resonances associated with the natural isotopic abundancies of chlorine in DCE. Full calculated anharmonic infrared energies for each isomer are shown in Table 6, Table 7, and Table 8. Fermi resonance affects were calculated for ^{35}Cl – ^{35}Cl, ^{35}Cl – ^{37}Cl and ^{37}Cl– ^{37}Cl isotope combinations which can be seen in Table 4, these Fermi resonance effects on the b_u CH bend (v_{10}) can be seen in Figure 41 where there are two distinct peaks and a shoulder evident at 1202.785cm^{-1}. The Fermi resonance affect has pushed the peaks higher due to the ^{35}Cl – ^{37}Cl and ^{37}Cl– ^{37}Cl isotopes, while the ^{35}Cl – ^{35}Cl has been pushed to a lower wavenumber due to the interaction. This has resulted in a clearly resolved peak that shows isotope contribution to the bu CH bend (v_{10}), despite the increased linewidth.

Peaks from scan	Calculated b_u CH bend (v_{10})	Fermi combined ag CCCl deform (v_5) and a_g CCl stretch (v_4)	Chlorine Isotope Contribution
1203.285 cm^{-1}	1203.738 cm^{-1}	1195.034 cm^{-1}	^{35}Cl – ^{37}Cl
1201.030 cm^{-1} (shoulder)	1202.785 cm^{-1}	This combination is not affected by Fermi resonance	^{37}Cl– ^{37}Cl
1196.841 cm^{-1}	1193.541 cm^{-1}	1202.785 cm^{-1}	^{35}Cl – ^{35}Cl

Table 4: (v_{10}) observed peaks in solid DCE with no argon present with calculated using Gaussian 09, isotope contribution.

$^{35}Cl - {}^{35}Cl$	Fermi resonances ---------- I J + K Freq.Diff. Reduced Cubic Const. PT2-Variat.Diff. 1 3 3 -12.725 131.243 -562.388 5 10 8 -0.954 18.919 -2305.641 2 Active Fermi resonances over 2
$^{35}Cl - {}^{37}Cl$	Fermi resonances ---------- I J + K Freq.Diff. Reduced Cubic Const. PT2-Variat.Diff. 1 3 3 -12.646 131.261 -573.440 5 10 8 6.832 -18.661 5.941 2 Active Fermi resonances over 2
$^{37}Cl - {}^{37}Cl$	Fermi resonances ---------- I J + K Freq.Diff. Reduced Cubic Const. PT2-Variat.Diff. 1 3 3 -12.552 131.280 -586.722 1 Active Fermi resonances over 1

Table 5: Calculated Fermi resonances for DCE isomer from Gaussian 09, states labelled differently to NIST look at appendix for full anharmonic infrared energies

Matrix Isolation Infrared Spectroscopy

Due to the correlation between the solid deposited on the windows of the infrared cell and the deviated baseline an argon matrix isolation experiment was also performed. This showed very interesting results. When the scan was run at 20 K after deposition the scans showed very sharp and well defined peaks at 3110.634 cm^{-1} (Figure 44), with 3106.549 cm^{-1} and 3104.337 cm^{-1}. The 1202.294 cm^{-1} peak (Figure 45) with lesser peaks at 1201.872 cm^{-1} and 1201.412 cm^{-1}. Due to the very low concentration of DCE that is deposited (Ar:DCE approx. 1000:1) this resulted in well-defined peaks at the 906.576 cm^{-1} and 821.804 cm^{-1} comparatively to the supercritical environment.

However, that distinctive baseline deviation difference noticed with a deposition of solid trans-1,2-dichloroethylene onto the infrared cell is missing from the solid matrix. This might be due to the very low temperature, 20 K, which the cell is sitting at reducing a potential interaction that was able to occur at 151 K. The matrix was allowed to warm up slowly, cryo-cooler turned off and no heating, and another scan run at 117 K. This showed that the DCE had disappeared across all wavenumbers (Figure 47 and Figure 48). Although the well-defined peaks due to isolated DCE molecules had disappeared at this temperature there was still solid DCE on the matrix isolation window. All argon is removed at this temperature having sublimed off at lower temperatures into the high vacuum. The peaks had typical symmetric lineshapes for the solid phase. In all but one case (ν_{10}, CH bend) the isotope splitting was not resolved due to the broad linewidth. In the case of the CH bend around 1200 cm^{-1} two peaks attributable to the effects of Fermi resonance can be seen. Interestingly the argon matrix environment is

sufficiently perturbing, for all the isotopic species present, to either the fundamental CH bend or the (two states) interacting by Fermi resonance with it that they are no longer shifted apart in the same manner.

Fano Resonance

The asymmetric lineshapes exhibited in some of the spectra appear to be classic examples of a Fano lineshape (Fano, 1961). A Fano Resonance is an interaction where a discrete state couples to a background continuum process that results in an asymmetric line shape (Figure 29). Some conditions must be met, including the resonant energy must be within the continuum's energy range. In the infrared cell a process has occurred which has resulted in a deposit of a thin layer, possibly a monolayer, of trans-1,2-dichloroethylene onto the window. This has allowed a situation to develop where the excitation of the trans-1,2-dichloroethylene by the infrared is occurring at the same time as a background scattering process is occurring through a continuum of states. By locking the trans-1,2-dichloroethylene in a solid argon matrix this continuum is blocked and the asymmetric line shape does not occur. This appears to be an unusual process for infrared spectroscopy however it is seen and used in surface-enhanced raman scattering (SERS). Further work, including modelling of the lineshapes observed, additional temperature dependence experiments and changing the nature of the molecule involved are in progress to try to understand the origin of the continuum involved, but are outside the scope of this thesis.

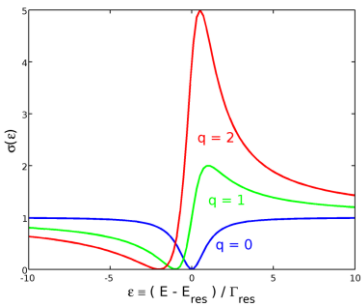

Figure 29: Plot of scattering cross-section versus normalized energy for various values of the parameter q illustrating the asymmetric Fano line-shape.

https://en.wikipedia.org/wiki/Fano_resonance#/media/File:Fano-resonance-scs.png

Infrared Spectra

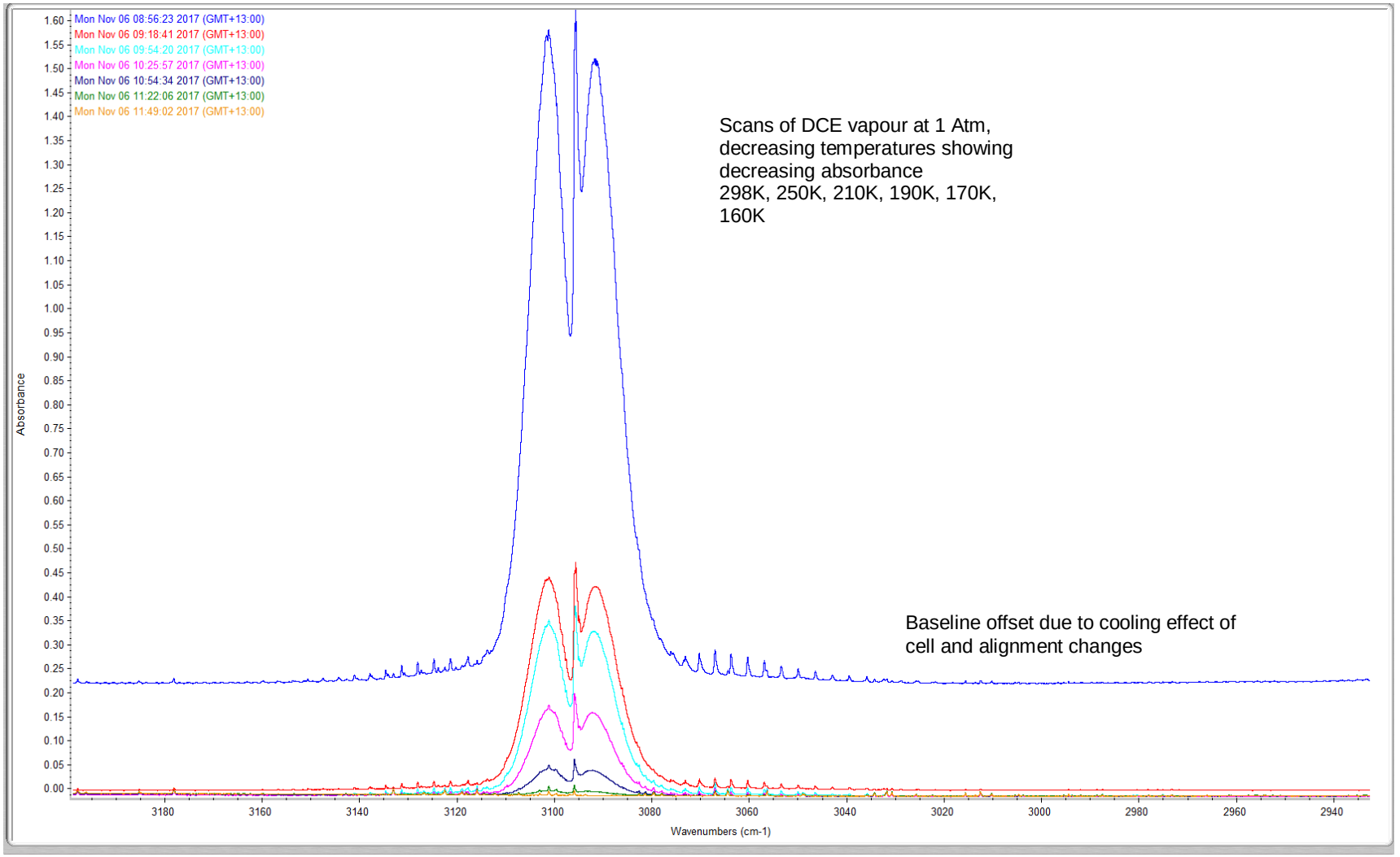

Figure 30: IR scans showing absorbance decrease as temperature decreases 298 K to 160 K at b_u CH stretch (v_9)

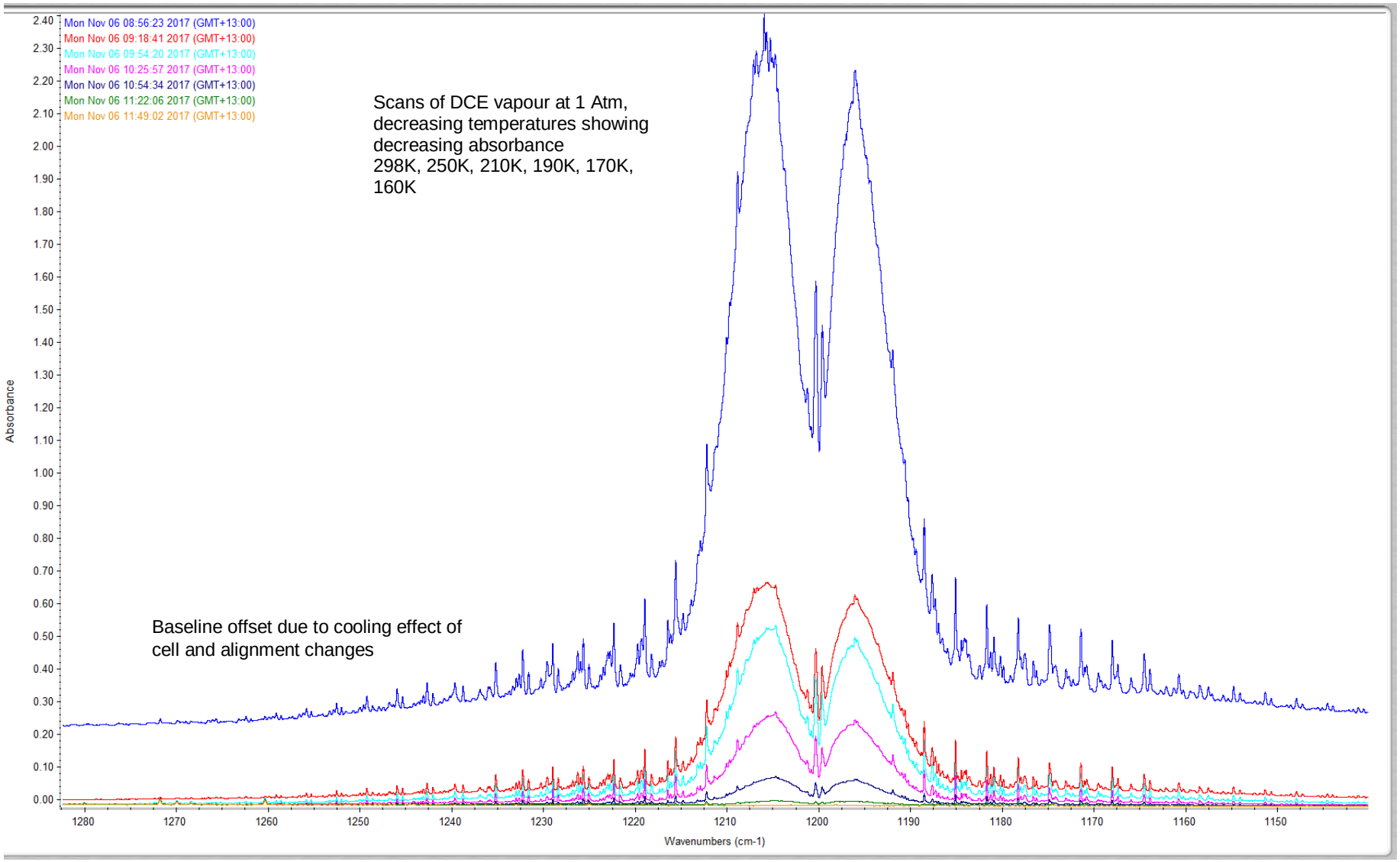

Figure 31: IR scans showing absorbance decrease as temperature decreases 299 K to 160 K at b_u CH bend (v_{10})

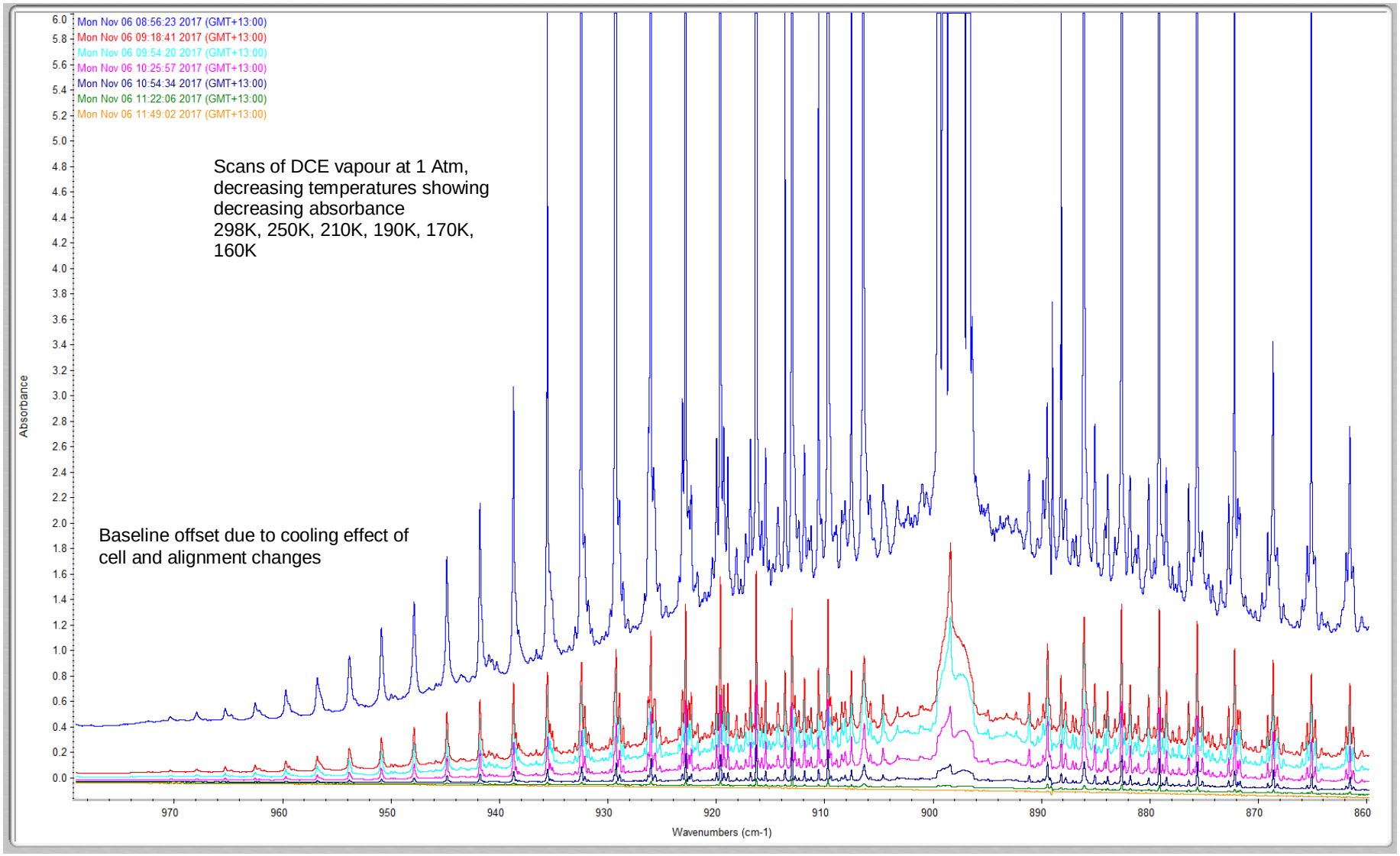

Figure 32: IR scans showing absorbance decrease as temperature decreases 299 K to 160 K at CH bend (v_6)

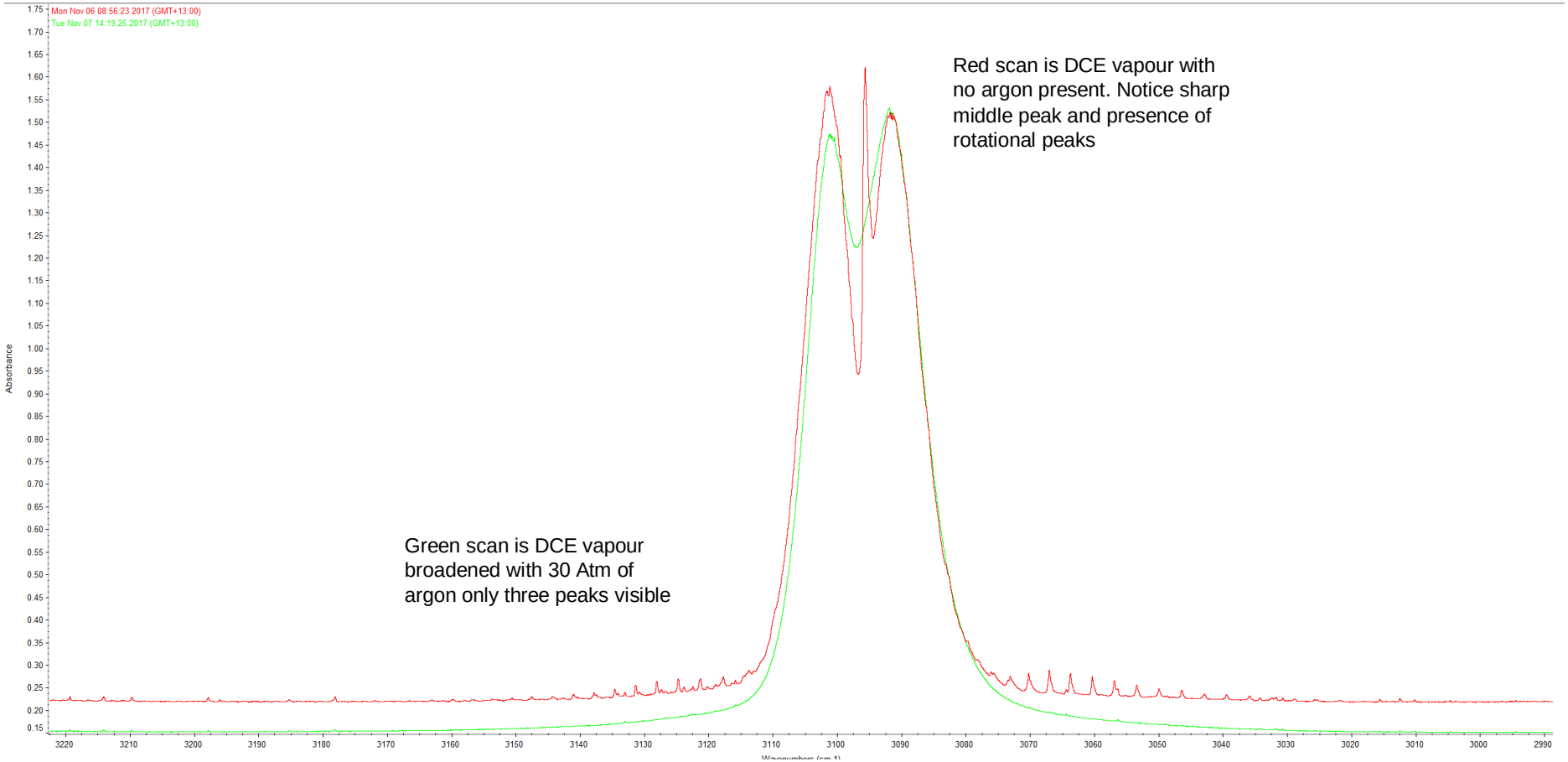

Figure 33: IR scan of DCE vapour compared to high pressure broadened peak at b_u CH stretch (v_9)

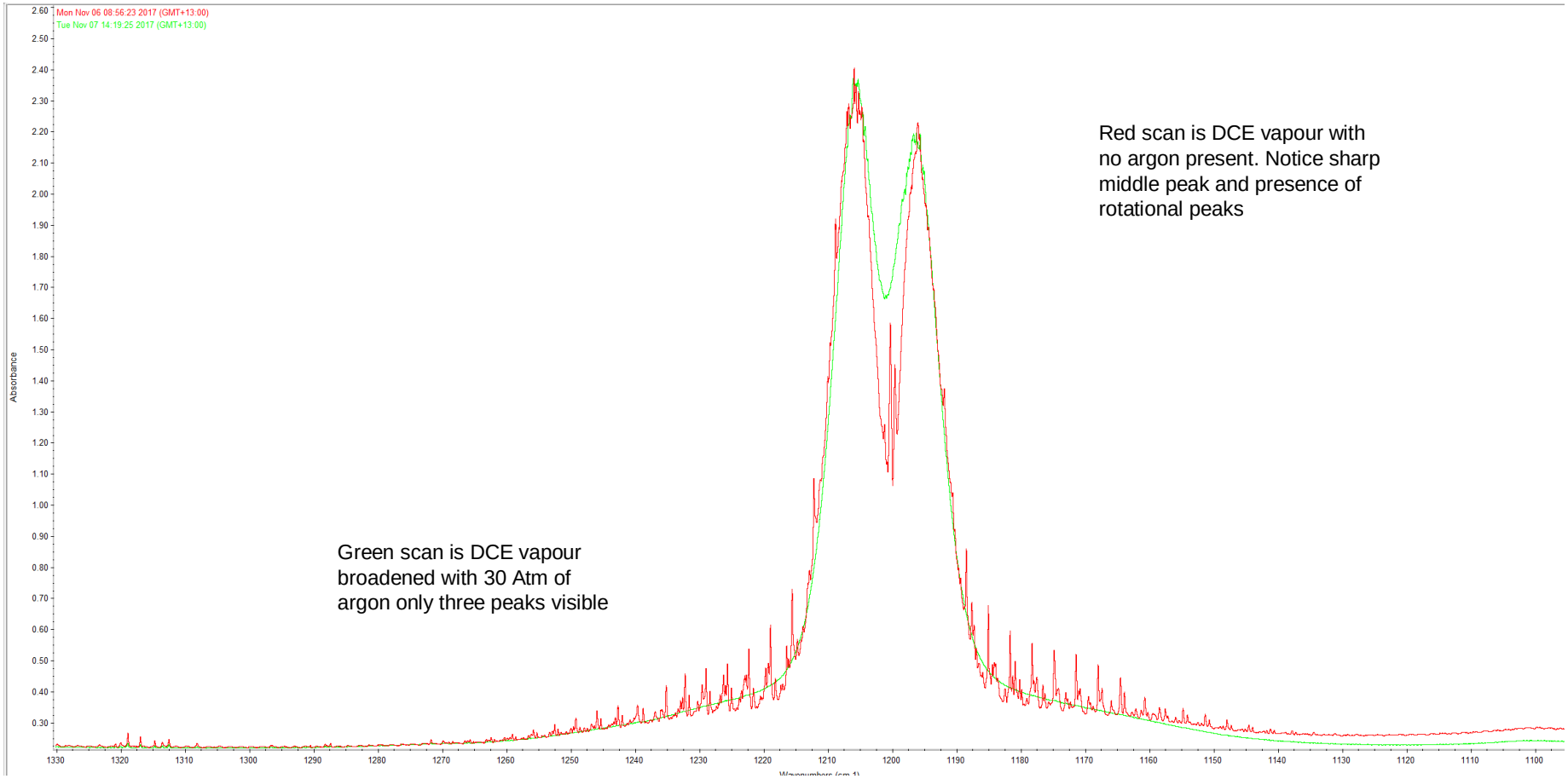

Figure 34: IR scan of DCE vapour compared to high pressure broadened peak at b_u CH bend (v_{10})

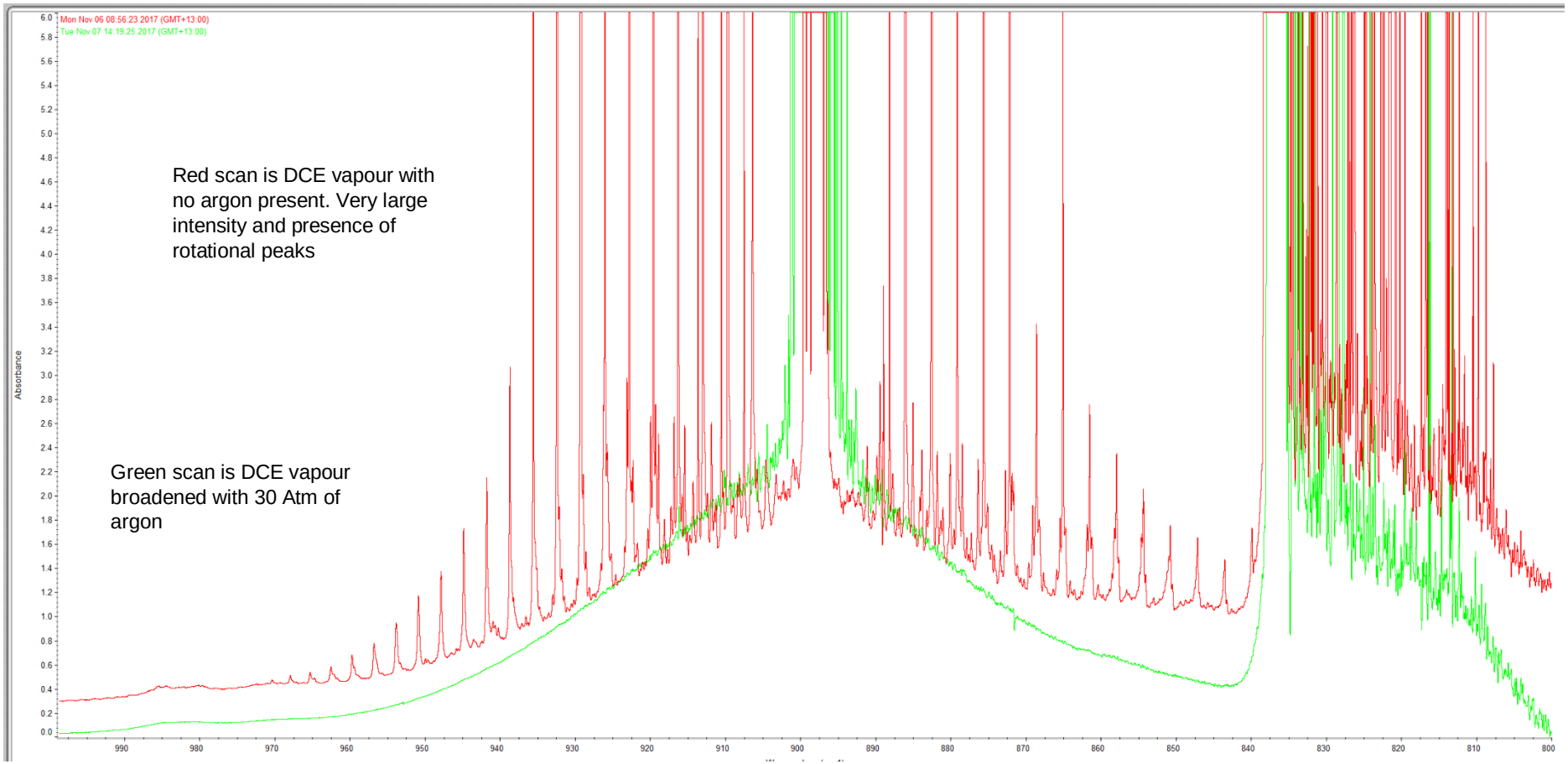

Figure 35: IR scan of DCE vapour compared to high pressure broadened peak at CH bend (v_6)

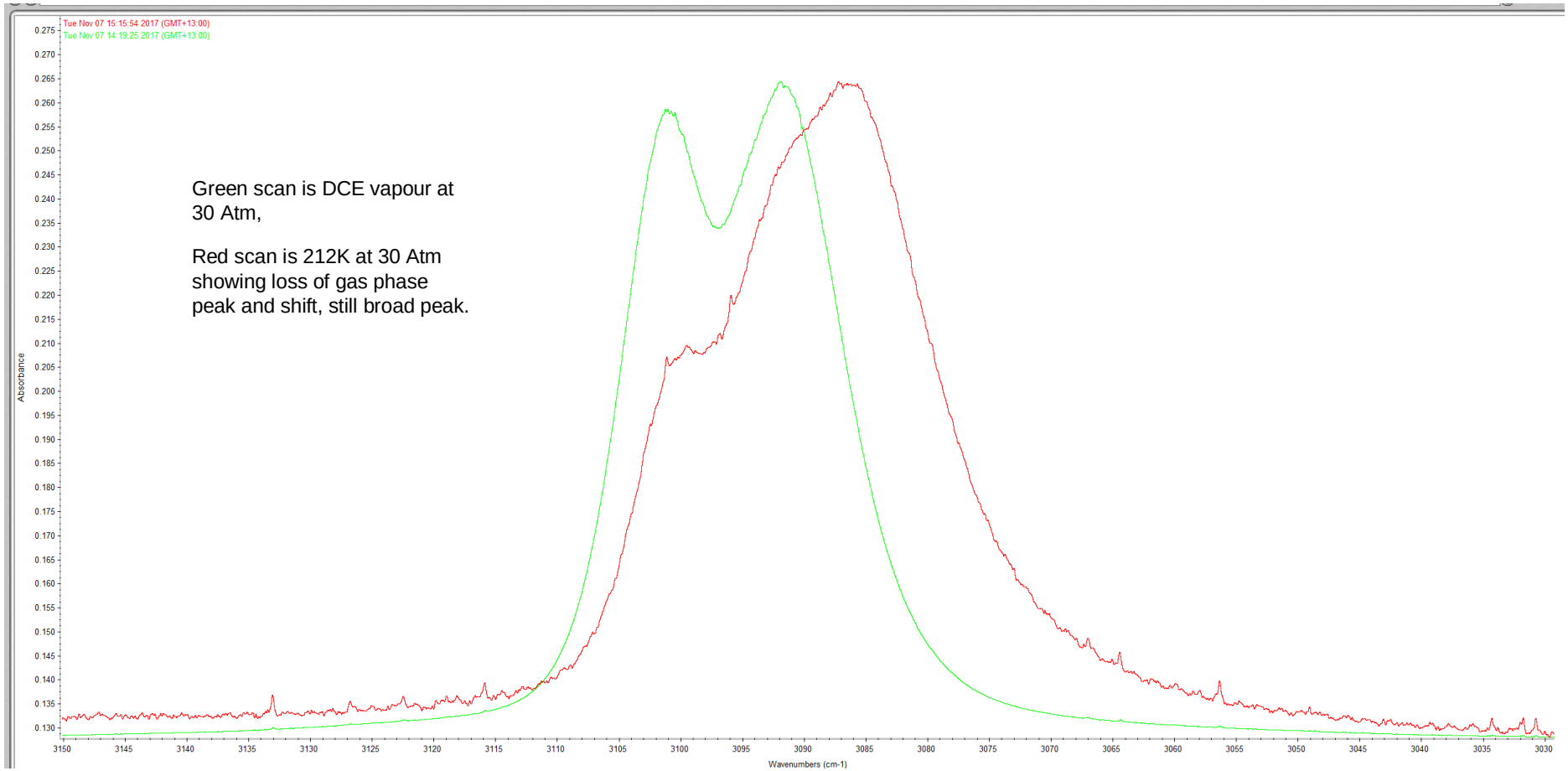

Figure 36: Comparison of liquid DCE formed at 212 K with broadened gas phase DCE at b_u CH stretch (v_9)

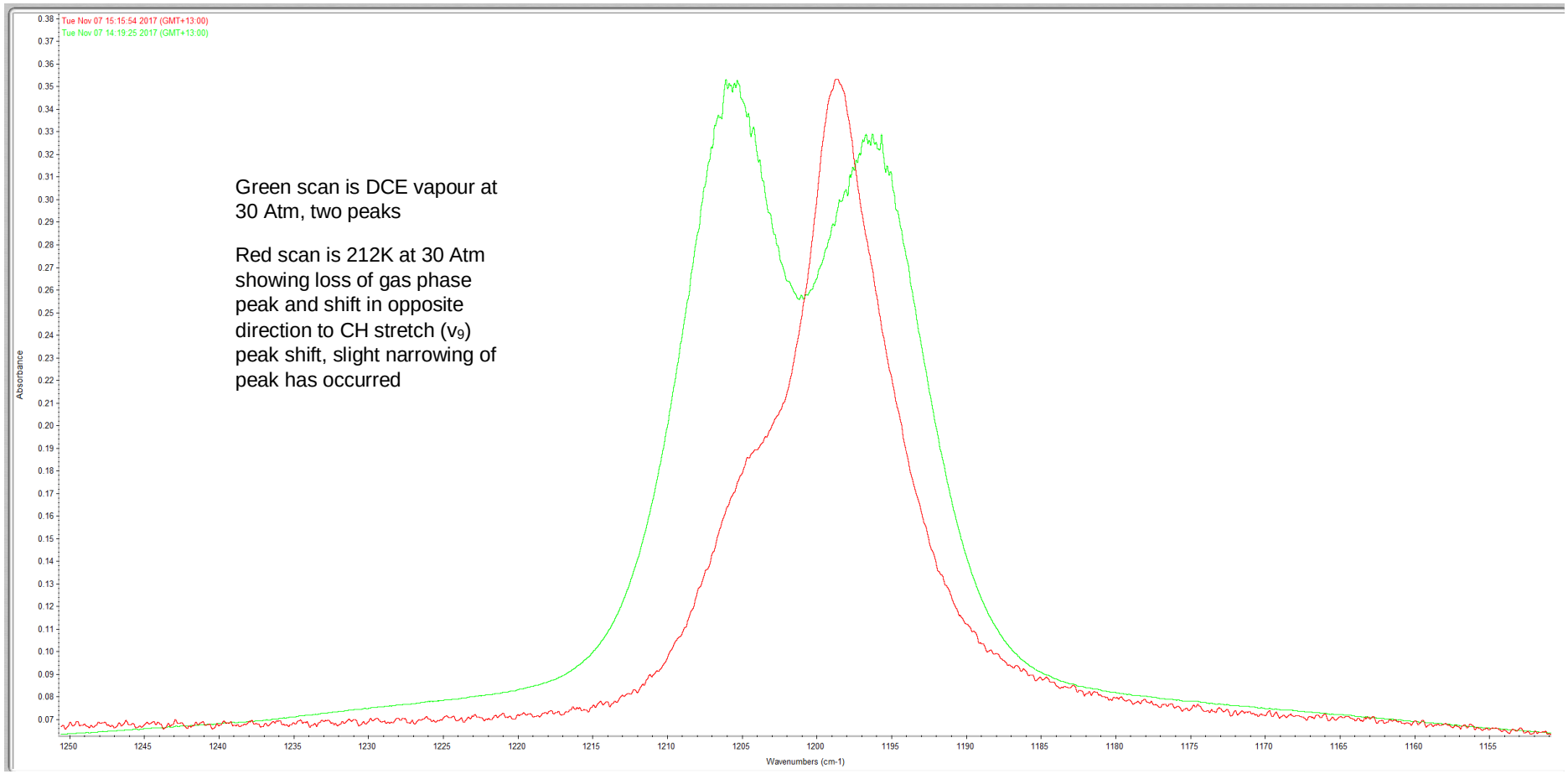

Figure 37: Comparison of liquid DCE formed at 212 K with broadened gas phase DCE at b_u CH bend (v_{10})[1]

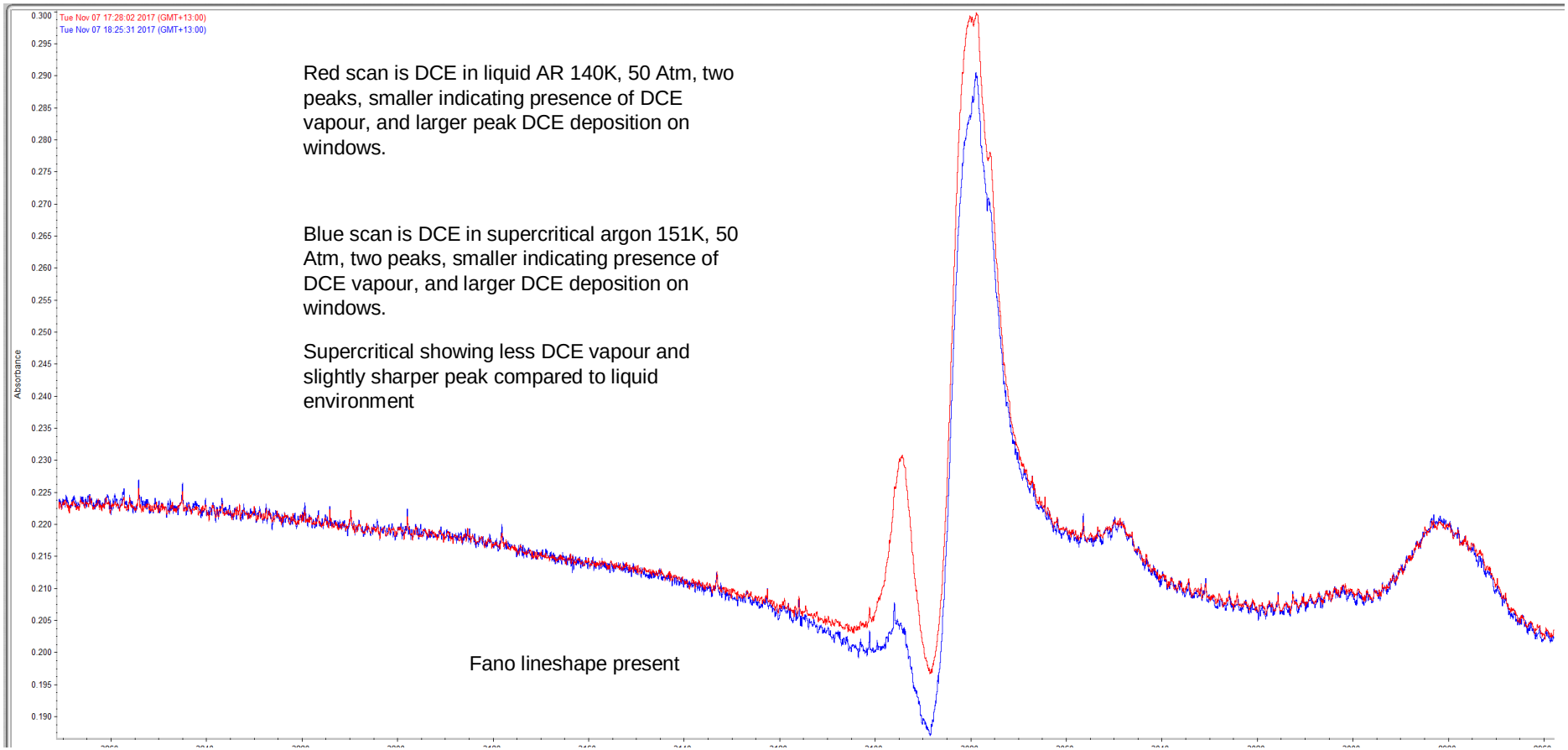

Figure 38: DCE in liquid and supercritical argon at b_u CH stretch (v_9)

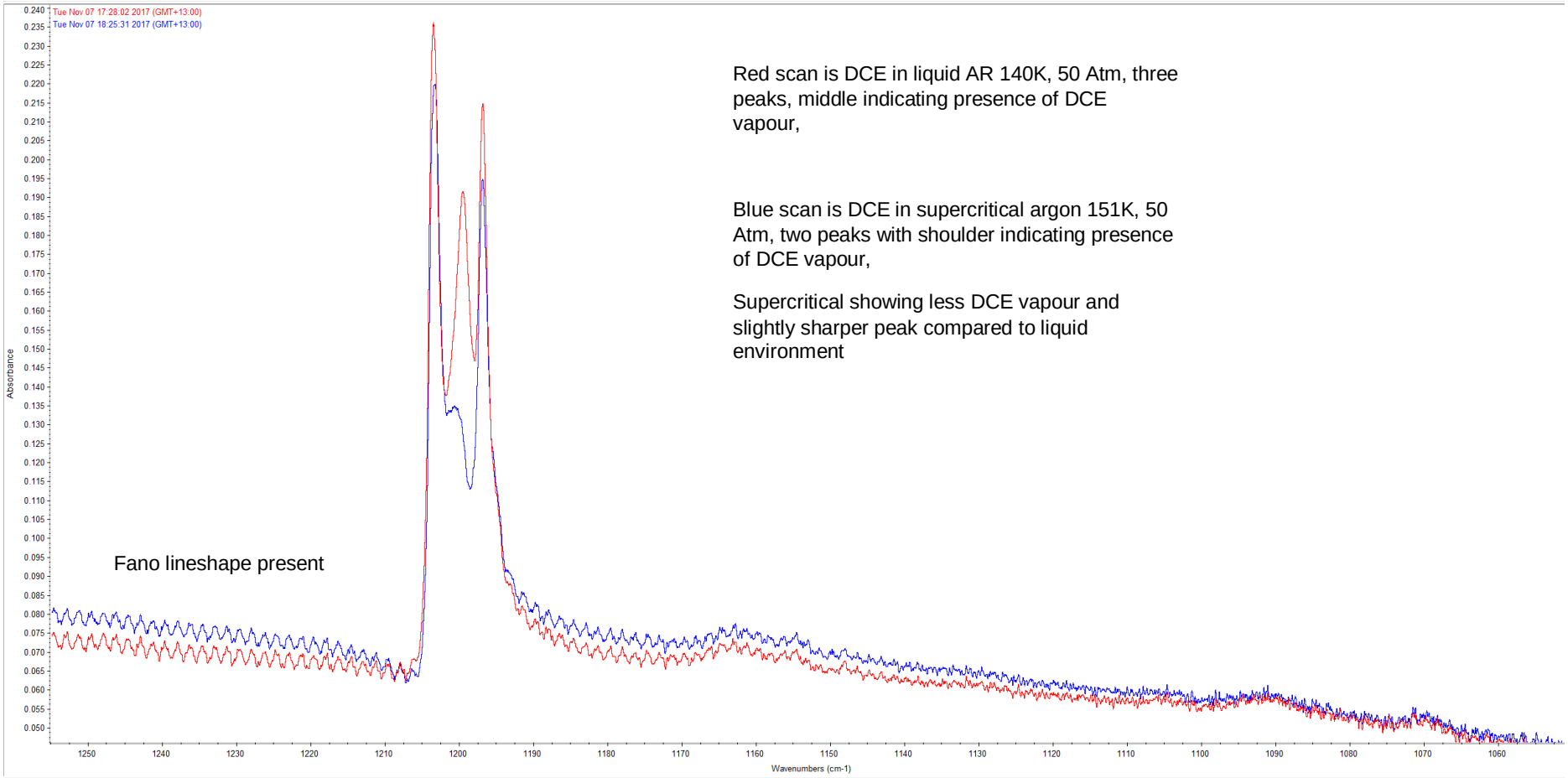

Figure 39: DCE in liquid and supercritical argon at b_u CH bend (v_{10})

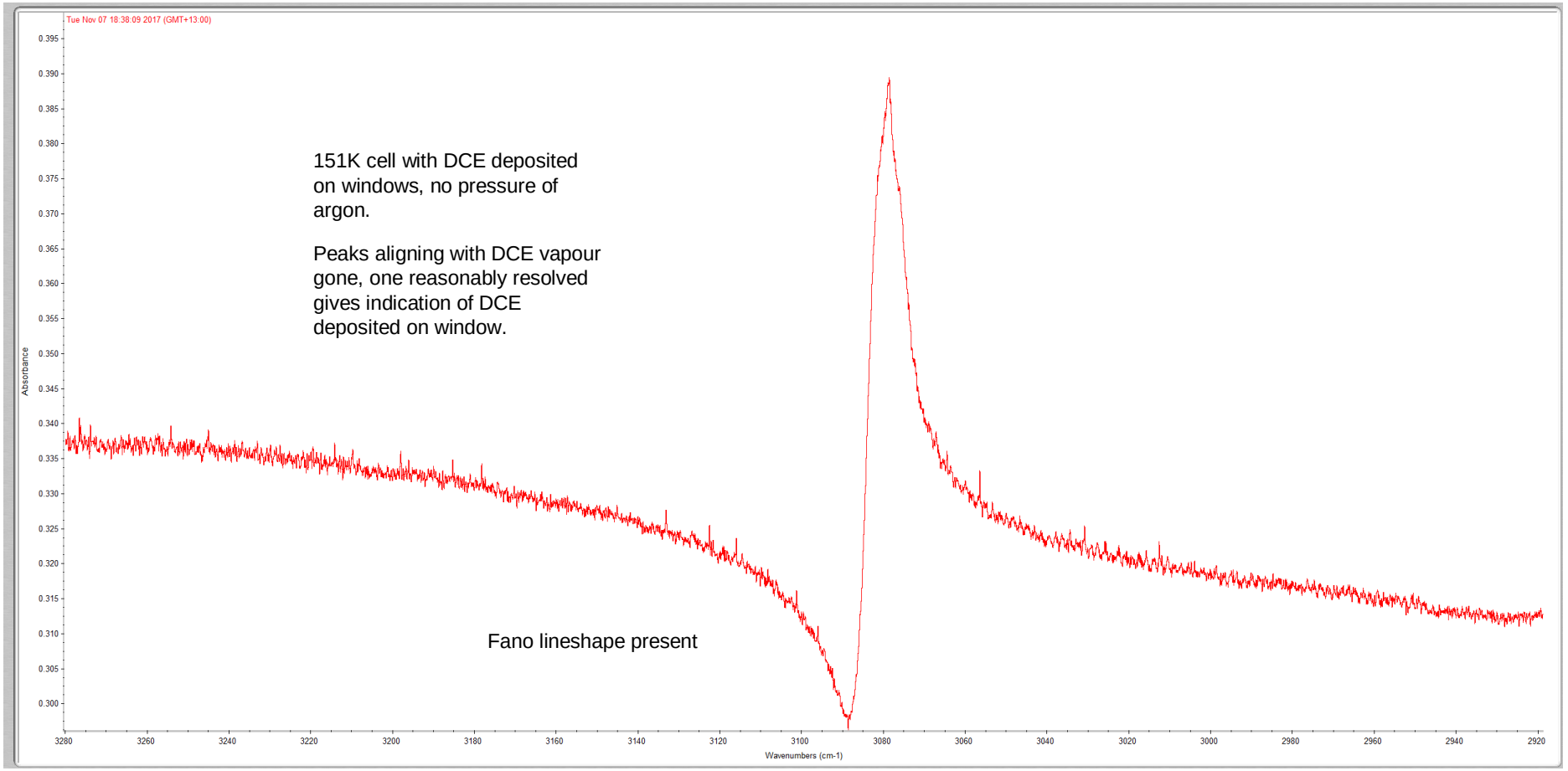

Figure 40: IR scan of cell at 151 K with solid DCE and residual argon removed b_u CH stretch (ν_9)

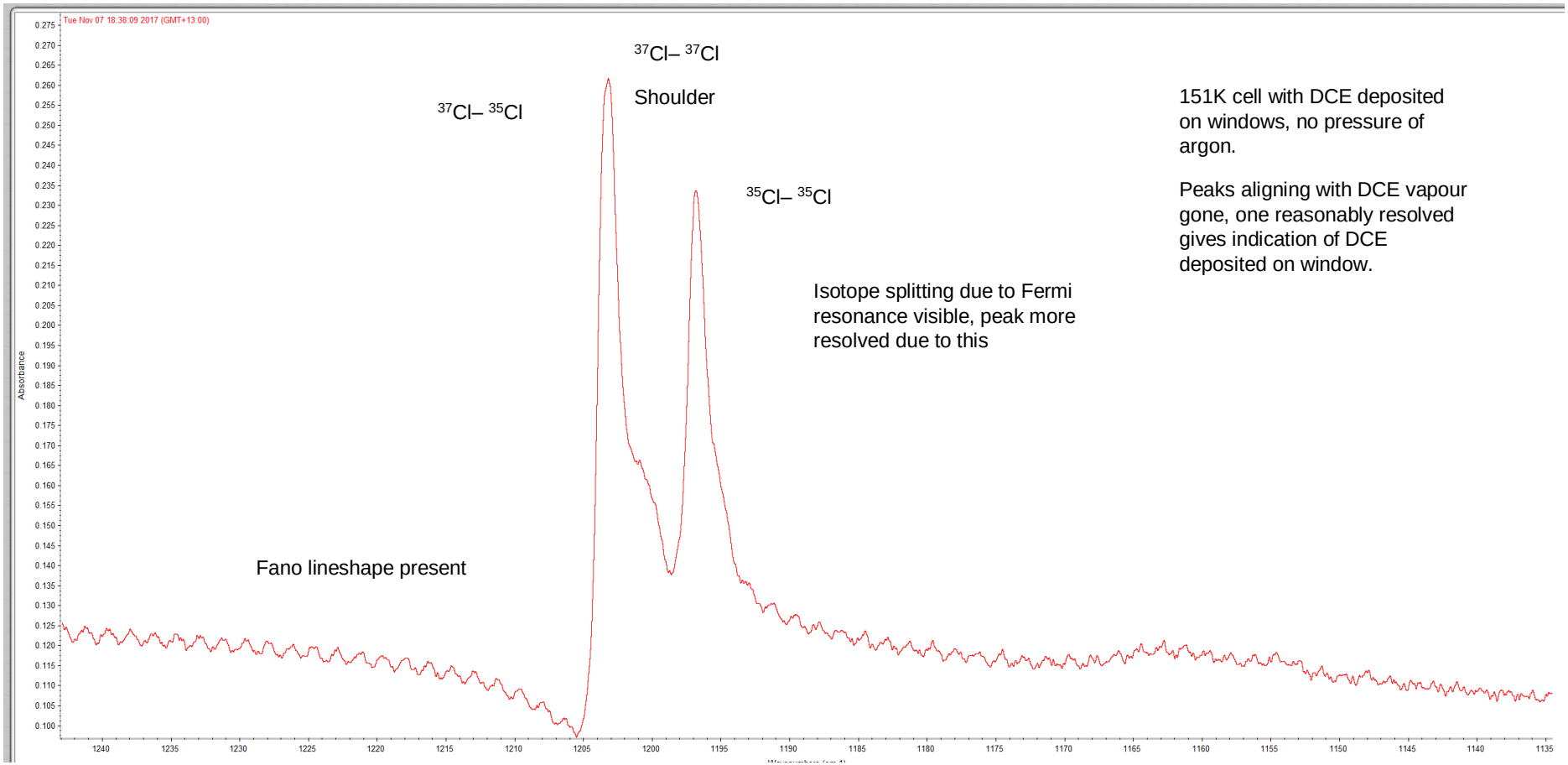

Figure 41: IR scan of cell at 151 K with solid DCE and residual argon removed at b_u CH bend (v_{10})

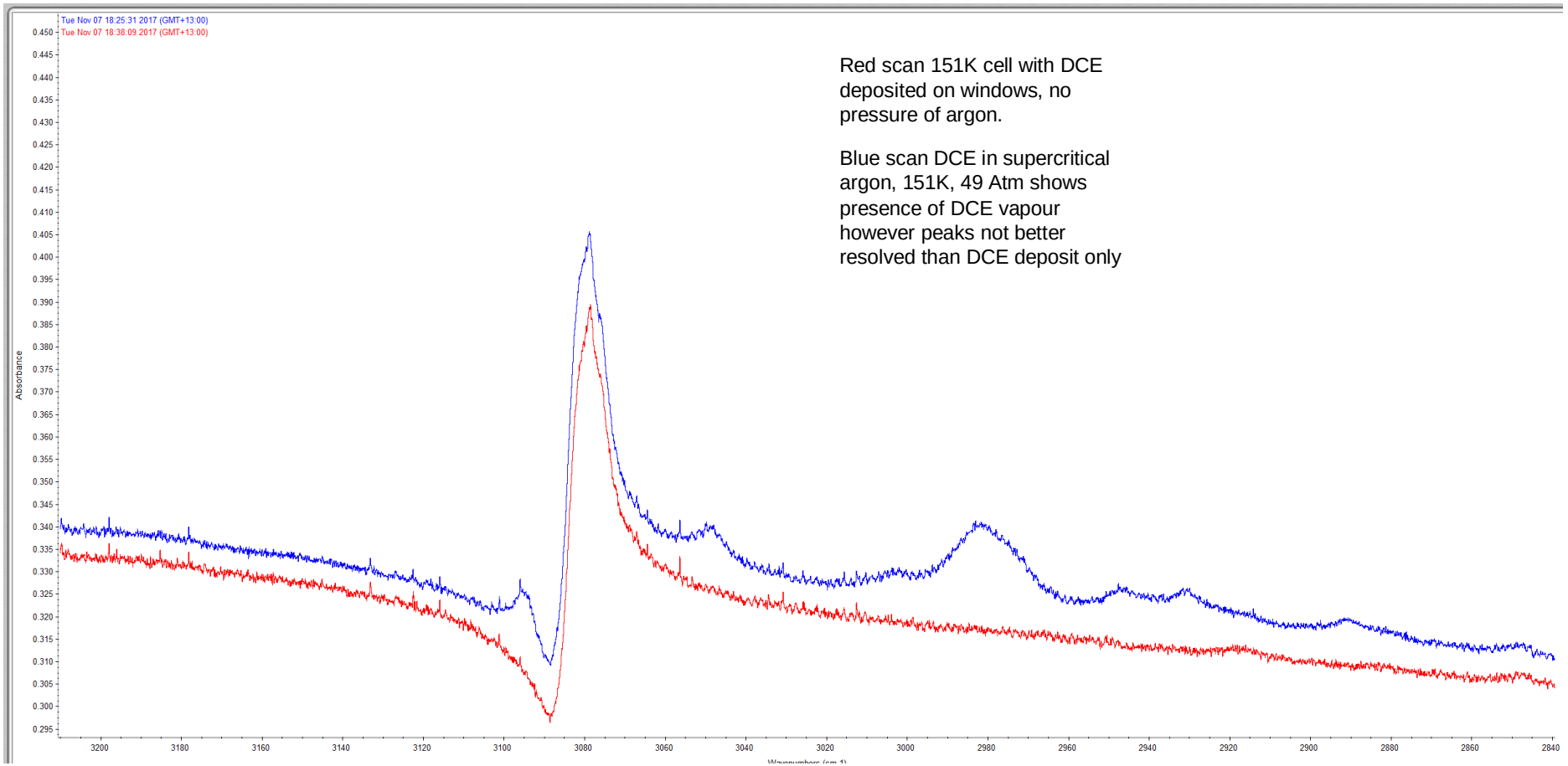

Figure 42: IR comparison of DCE in supercritical argon and solid deposition on cell windows at b_u CH stretch (v_9)

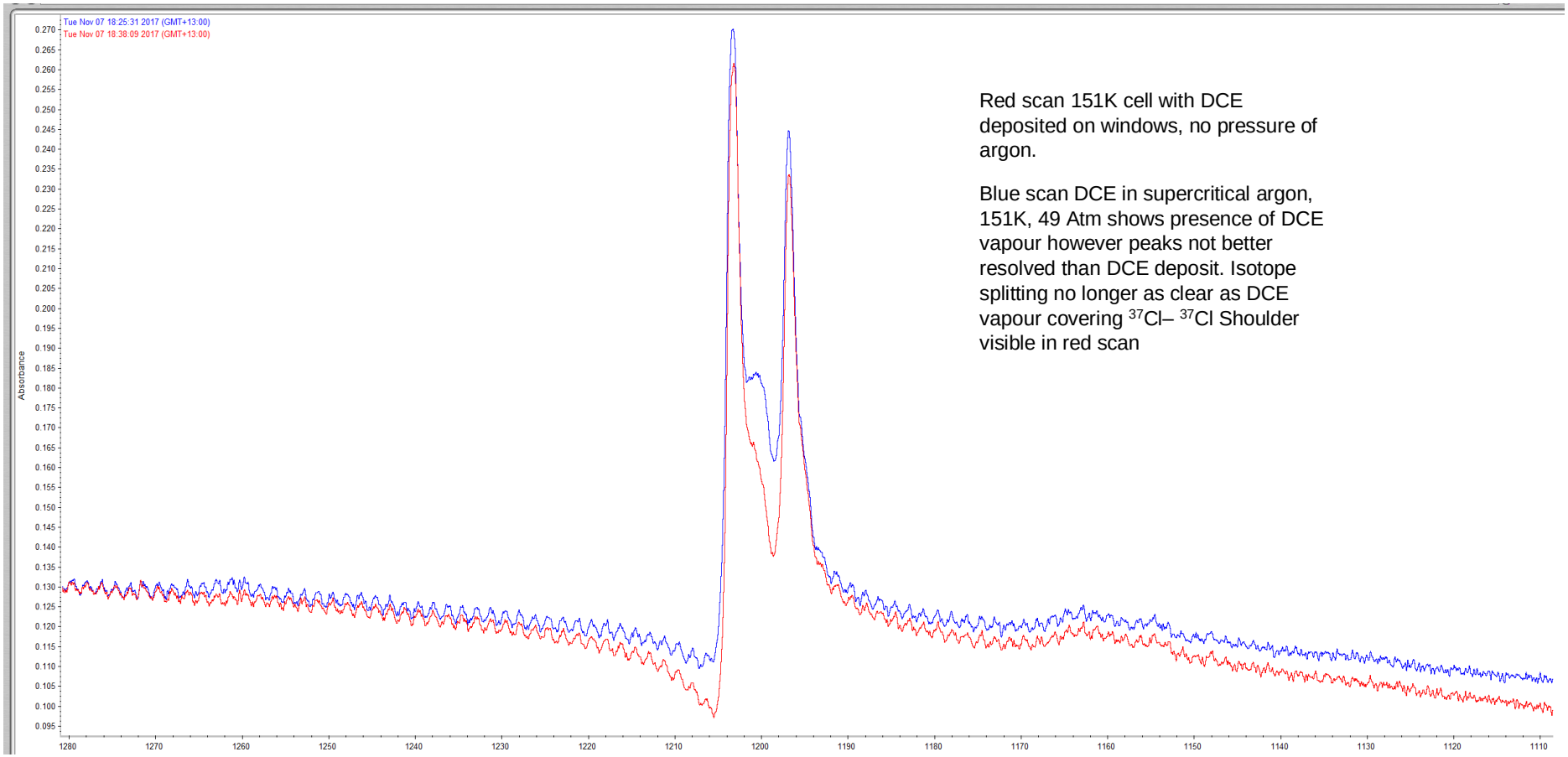

Figure 43: IR comparison of DCE in supercritical argon and solid deposition on cell windows at b_u CH bend (v_{10})

Matrix Infrared Spectrums

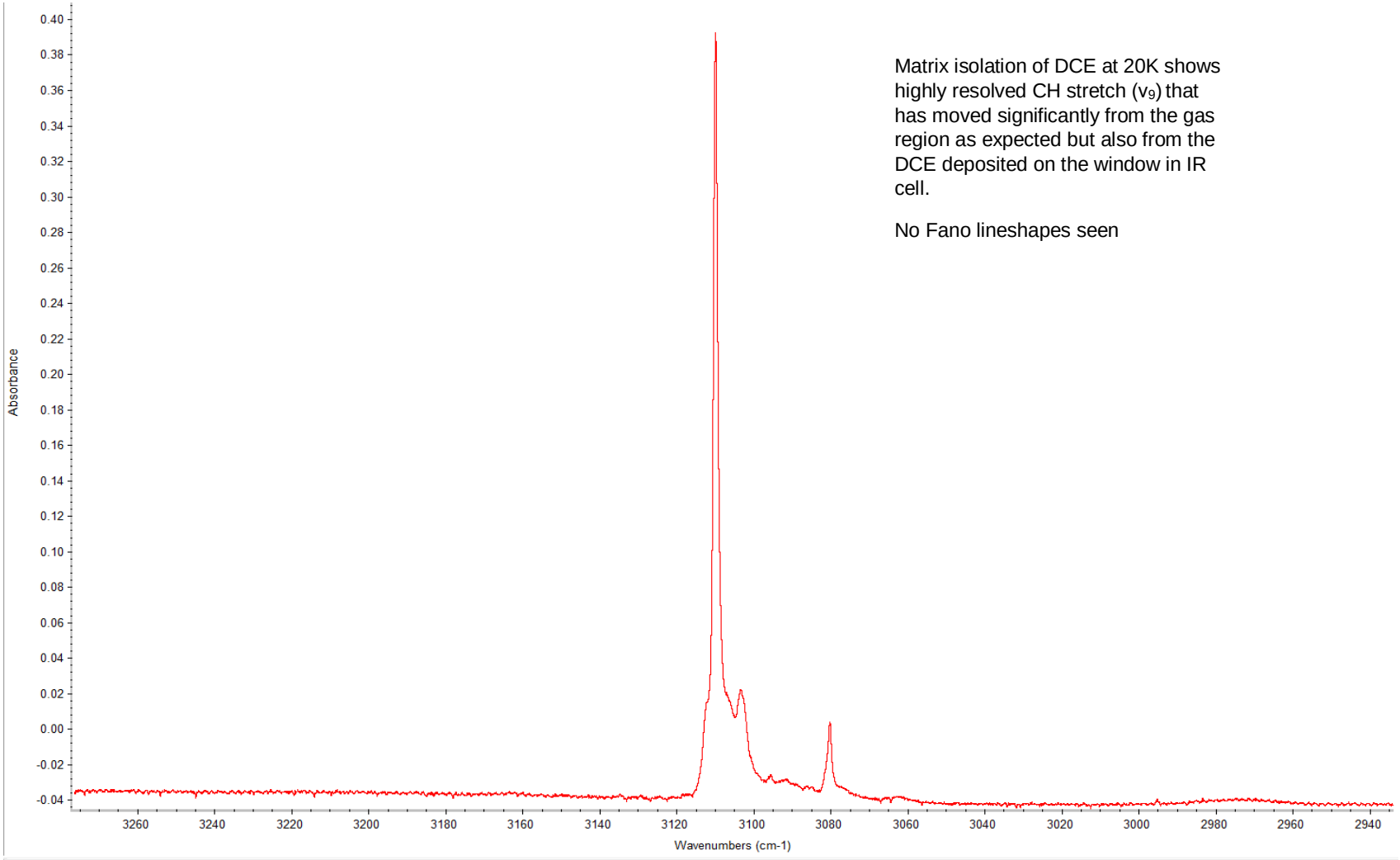

Matrix isolation of DCE at 20K shows highly resolved CH stretch (ν_9) that has moved significantly from the gas region as expected but also from the DCE deposited on the window in IR cell.

No Fano lineshapes seen

Figure 44: DCE at 20 K in solid argon at b_u CH stretch (ν_9)

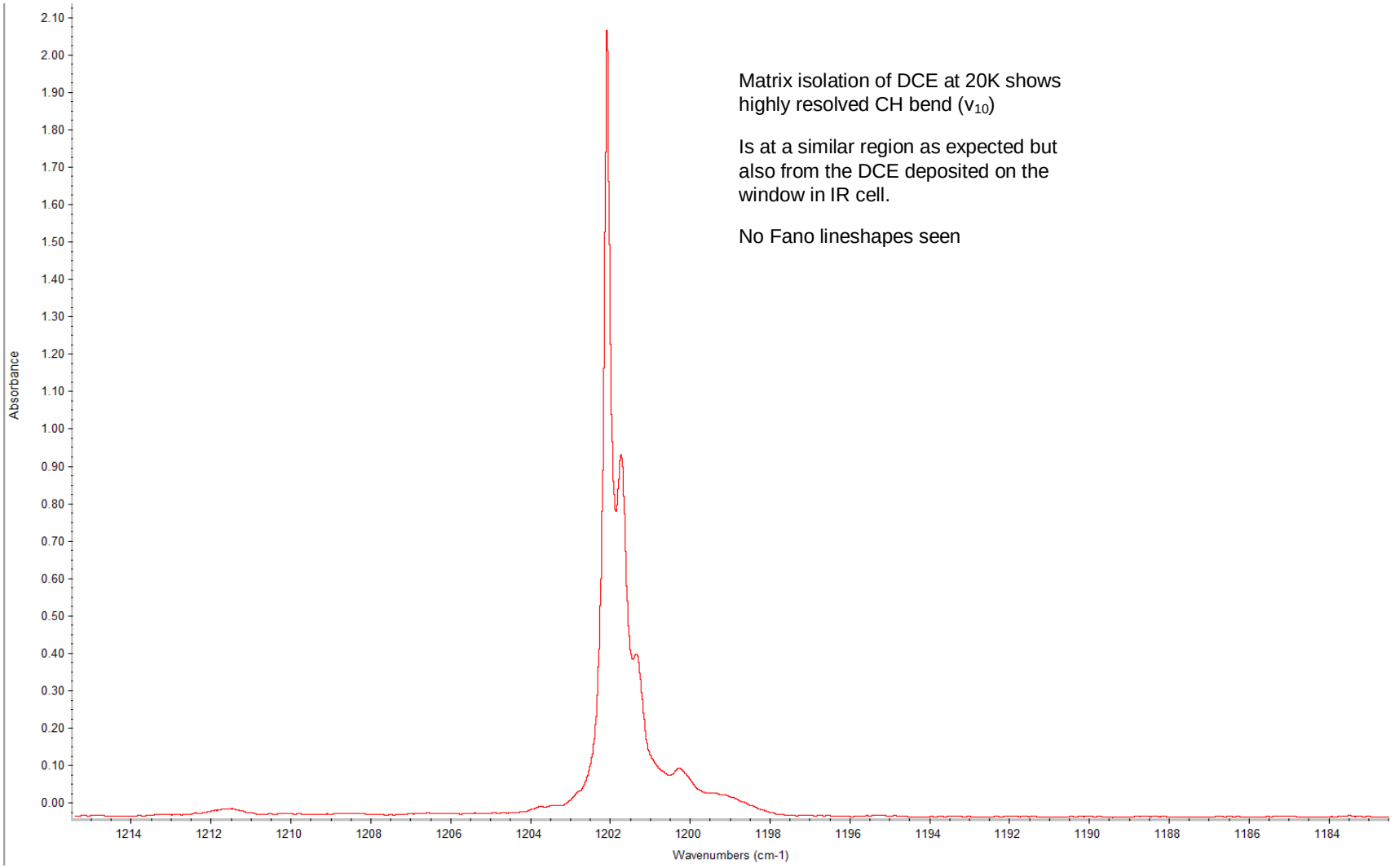

Figure 45: DCE at 20 K in solid argon at b_u CH bend (v_{10})

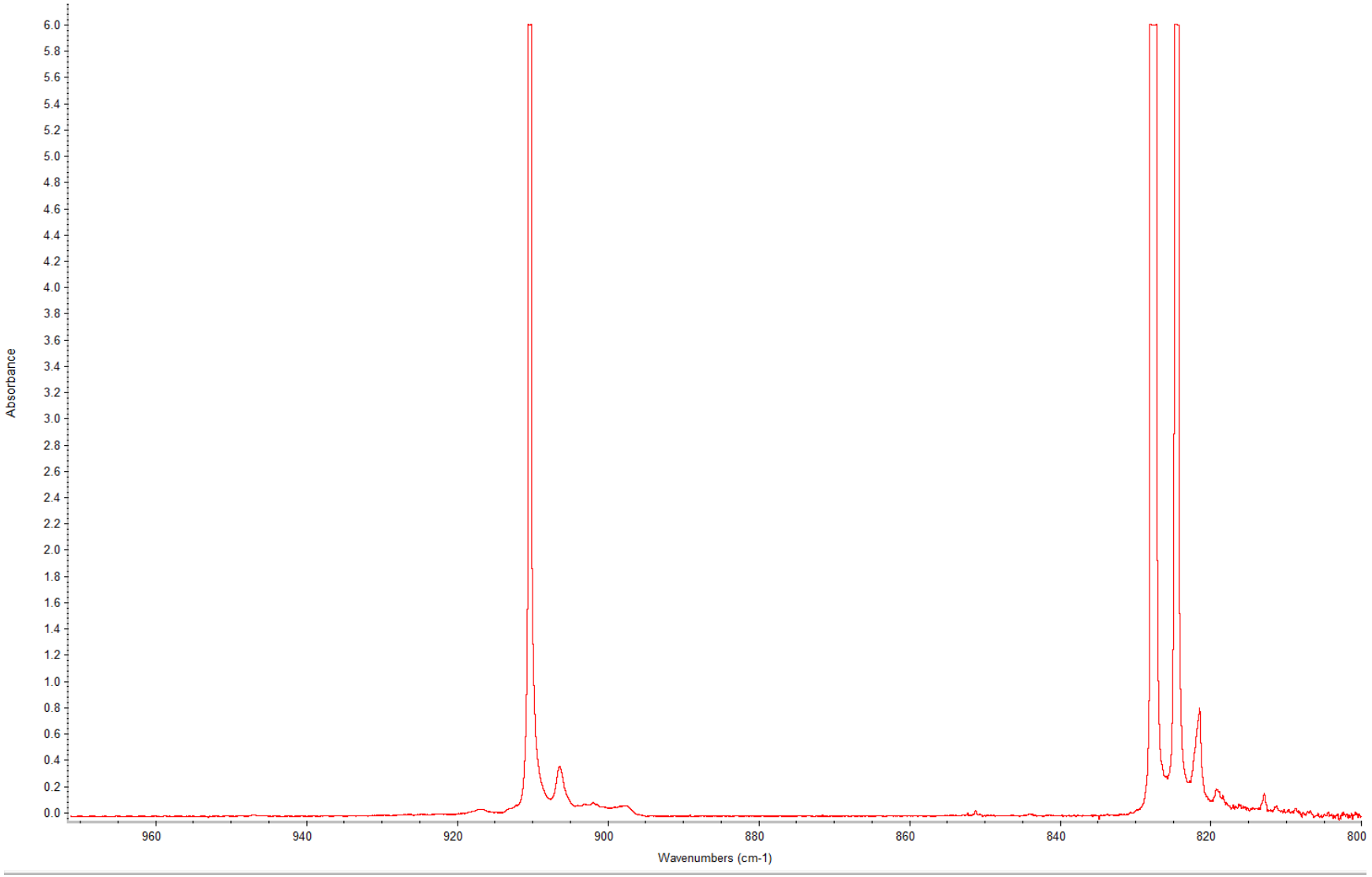

Figure 46: DCE at 20 K in solid argon at CH bend (v_6)

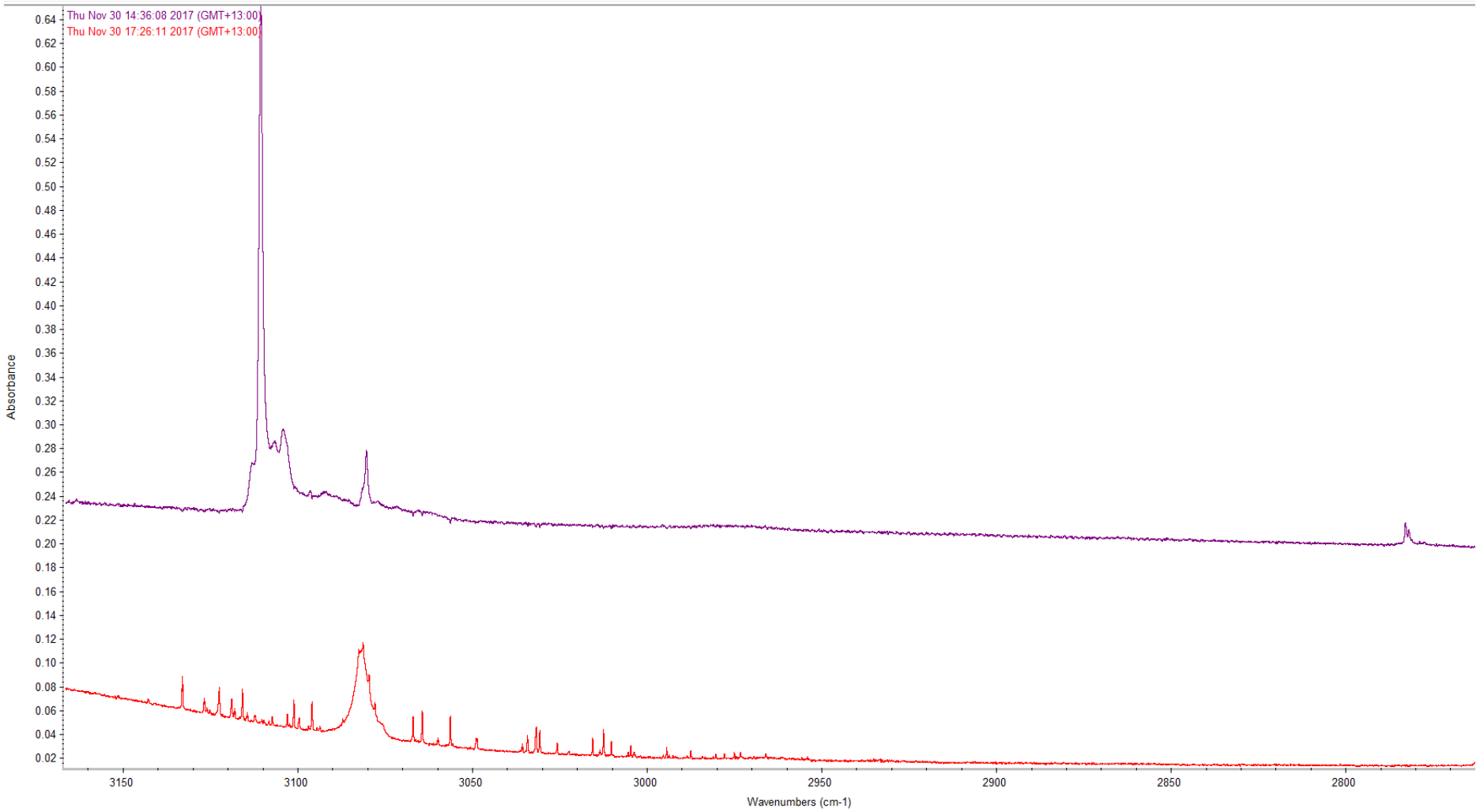

Figure 47: Comparison of matrix scan at 8 K vs 117 K, visible loss of DCE at b_u CH stretch (v_9). Sharp peaks in the lower spectrum are atmospheric absorptions due to a drift in the purge conditions during the three hours between scans.

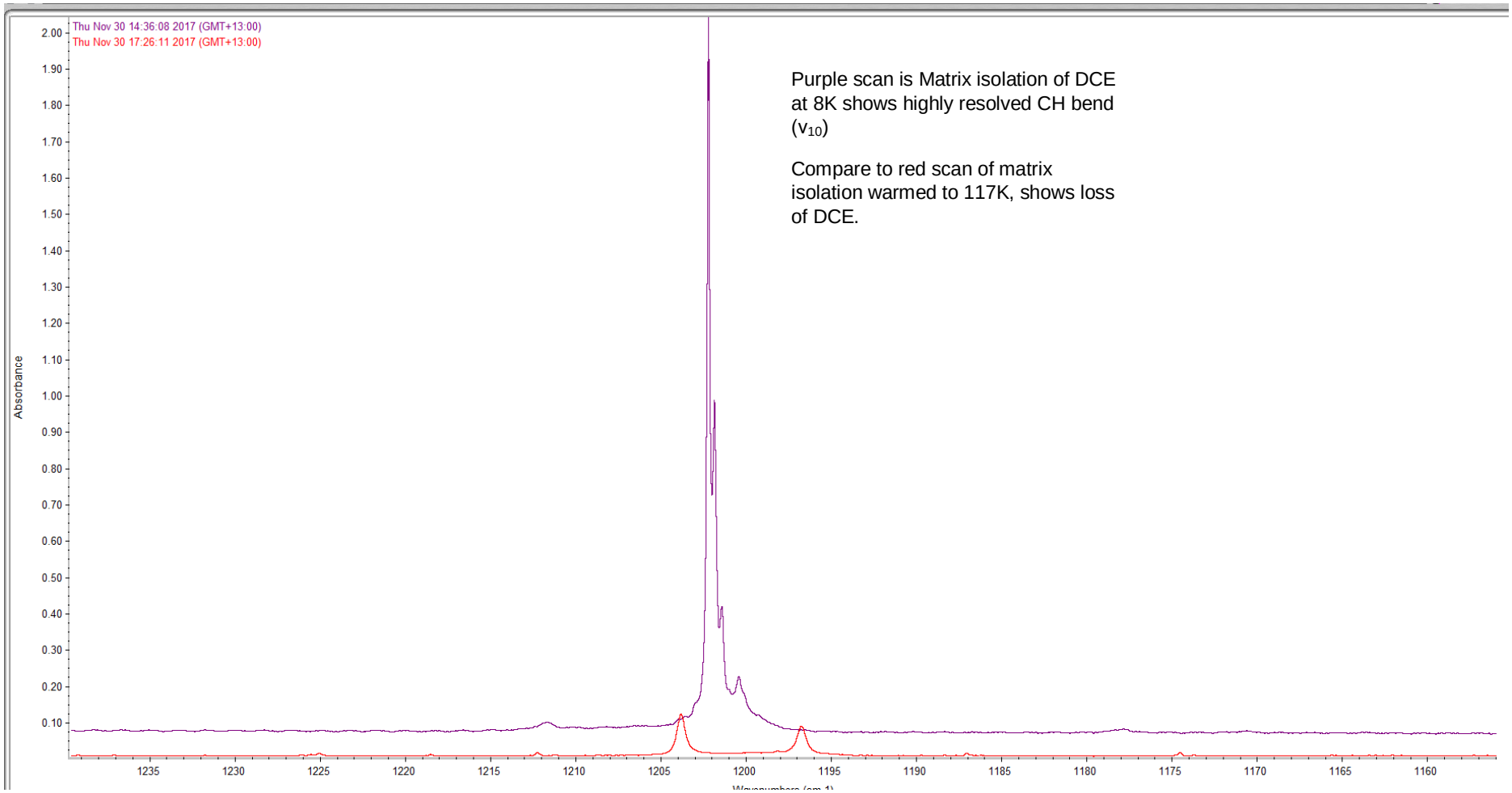

Figure 48: Comparison of matrix scan at 8 K vs 117 K, visible loss of DCE at b_u CH bend (v_{10})

Conclusion

In conclusion there has been a large amount of ground covered in the investigation of the supercritical properties of argon and its interaction with trans-1,2-dichloroethylene (DCE). It has resulted in a robust cell design that can continue to be used for other analysis and some interesting Fano resonance lineshapes that need much more investigation.

The initial cell construction encountered many obstacles, specifically around the sealing of the cell unit against the high pressures required to reach the supercritical point of argon. The end result of using indium foil was not ideal due to its toxicity and the general inability to remove the initial quartz windows without breaking them once in place, however it has proved to be the most robust sealing gasket. The small scale that the ultraviolet-visible spectrophotometer sample compartment required did cause some frustration and limitations, again once the cell was constructed and aligned it was very robust and stable in the instrument allowing for multiple measurements. The biggest hurdle encountered was the sealing of the windows without breaking them and the difficulty in leak checking for a cold, high pressure environment at room temperature. Though it was a long testing process a functional cell was designed that was robust and reproducible to be cycled multiple times before a significant leak occurred.

The relationship with supercritical argon and trans-1,2-dichloroethylene (DCE) was first seen in the initial UV-Vis cell and showed promise for the development of a molecular beam pulsed valve. The ultraviolet-visible (UV-Vis) was not

detailed enough to give much indication of the state that DCE was in as the conditions of argon changed. However, the strong pattern of absorbance decreasing with temperature until the supercritical point was reached where the absorbance of DCE spiked showed there was a strong solubility interaction occurring.

The design and development of the molecular beam pulsed valve has been the most fraught part of this process. Many design and testing hours were spent trying to achieve a functional a valve that pulsed when required and sealed firmly when not. Because the valve never worked ideally, the results obtained showed little progress in seeding the beam with DCE. This experimental pathway was hindered by several factors including; design limitations, materials accessibility and equipment limitations specifically the cryo-cooler and the difficulty in controlling the temperature across the whole valve. The possibility for future solutions to this technique still remains, however more specialist equipment and time is likely required to obtain reproducible results.

The advantage in the molecular beam pulsed valve pathway being restrictive was the push towards taking the lessons learned in the initial cell and improving the system to allow for infrared analysis. This second cell was much more multipurpose, with an improved design in the circular window bracing blocks. The window leaking issue that was a significant problem in the initial design is still present but more controllable. The addition of a third window allows for the cell

to undergo fluorescence and the external vacuum casing is able to fit into three different instruments.

The infrared analysis initially showed a great relationship to the UV-Vis absorbance reduction with reduction in temperature of the cell. However, as various states of argon were achieved, gas, liquid, and supercritical, there was a significant change in the CH stretch (v_9) and CH bend (v_{10}) positions and shapes observed. It is exciting to see these interactions happening in the cell and to allow for the investigation into how the supercritical argon is exactly interacting with the trans-1,2-dichloroethylene (DCE). The most interesting and surprising part observed is the appearance of the Fano resonance effect, in the liquid, supercritical and window deposit environment, this effect is not commonly see in the infrared environment.

The matrix environment provided another area of comparison to investigate just how DCE is interacting with argon. The matrix showed highly resolved peaks of DCE in its solid state, however the Fano resonance was not present. This showed that more investigation is required as the peaks shift for DCE in a solid matrix are substantially different to those observed in the deposit supercritical environment. The differences in the deposition of DCE in a matrix environment verses uncontrolled freezing of DCE to the window in the supercritical and liquid environments created more questions rather than answers.

This study has begun a much larger investigation into the interaction of supercritical argon as a solvent. Some areas of future research with supercritical

argon could cover a range of aspects. A continuance of this pathway with a detailed investigation will need to be undertaken to explain the Fano resonance effect that is being seen in DCE when interacted with a high pressure argon environment but not seen in the low pressure matrix. Then branch this out to a future study that could look at the interaction of less volatile compounds and fluorescence interactions and possibilities of both DCE and other molecules. Alongside this, the continued development in the direction of a functioning and robust molecular beam is required.

References

Besora, M., Carreon-Macedo, J.-L., Cowan, A. J., George, M. W., Harvey, J. N., Portius, P., . . . Towrie, M. (2009). A Combined Theoretical and Experimental Study on the Role of Spin States in the Chemistry of Fe(CO)5 Photoproducts. *Journal of American Chemical Society, 131*, 3583-3592.

Calladine, J. A., Vuong, K. Q., Sun, X. Z., & George, M. W. (2009). Recent advances in organometallic alkane and noble gas complexes. *81*(9).

Craig, N. C. (1998). A Complete Structure of trans-1,2-Dichloroethylene from High-Resolution Infrared Spectroscopy. *J. Phys. Chem. A,, 102*(34), 6745-6752.

Darr, J. A., & Poliakoff, M. (1999). New Directions in Inorganic and Metal-Organic Coordination Chemistry in Supercritical Fluids. *Chemical Reviews, 99*(2), 495-541.

Demtroder, W. (1996). *Laser Spectroscopy in Molecular Beams.* Germany: Springer.

Engel, T., & Reid, P. (2006). *Physical Chemistry* (4th Edition ed.). San Francisco: Pearson Benjamin Cummings.

Fano, U. (1961). Effects of Configuration Interaction on Intensities and Phase Shifts. *Physical Review, 124*(6), 1866-1878.

Guckert, J. R. (1990). Infrared laser photochemistry of trans-1,2-dichloroethylene. Evidence for a Cl atom chain reaction. *Laser Chem.*, 185-195.

Harrison, J. (n.d.). Part 3 Experimental Considerations. *Lecture 4: Molecular Beams*. Auckland: John Harrison.

He, G. Y. (1993). Distribution of Rotational States in Half-Collisions: 193-nm Photolysis of Dichloroethylene Isomers. *J. Phys. Chem.*, 2186-2193.

Ke, J., Su, W., Howdle, S. M., George, M. W., Cook, D., Perdjon-Abel, M., . . . Murray, R. W. (2009). Electrodeposition of Metals from Supercritical Fluids. *Proceedings of the National Academy of Sciences of the United States of America, 106*(35), 14768-14772.

Keller-Rudek, H. M. (2013). The MPI-Mainz UV/VIS spectral atlas of gaseous molecules of atmospheric interest. *Earth Syst. Sci. Data*, 365-373.

Liang, S., & Tilotta, D. C. (1998). Extraction of Petroleum Hydrocarbons from Soil Using Supercritical argon. *Analytical Chemistry, 70*(3), 616-622.

M. J. Frisch, G. W. (2017, December 21). Gaussian 09, Revision D.01,. Wallingford, Wallingford CT, United States of America.

McHugh, M. A., & Seckner, A. J. (1984). Xenon as a Supercritical Solvent. *88*.

Nishikawa, M. (20007). Behavior of charged species in supercritical heavy rare gas fluids. *76*.

Shimanouchi, T. (1972). *Tables of Molecular Vibrational Frequencies Consolidated Volume I.* National Bureau of Standards.

Appendix

Trans-1,2-dichloroethylene Calculated Isotopes Infrared Energies

for ^{35}Cl-^{35}Cl isotope
Anharmonic Infrared Spectroscopy
Units: Energies (E) in cm^-1
Integrated intensity (I) in km.mol^-1

Fundamental Bands				

Mode(Quanta)	E(harm)	E(anharm)	I(harm)	I(anharm)
1(1)	3260.358	3108.024	0	0.00005992
2(1)	3257.554	3128.985	16.98454678	14.15047954
3(1)	1636.542	1589.872	0	0.00003183
4(1)	1300.803	1277.144	0	0.00000641
5(1)	1220.735	1193.541	20.22245069	18.02189905
6(1)	934.442	912.987	54.44220429	54.20469141
7(1)	878.513	865.617	0	0.00000036
8(1)	861.816	846.878	110.1692094	112.1090263
9(1)	787.356	775.611	0	0.00001251
10(1)	359.872	355.892	0	0.00000072
11(1)	239.139	240.687	3.35671331	3.36349744
12(1)	217.69	217.307	0.20918182	0.22860134
Overtones				

Mode(Quanta)	E(harm)	E(anharm)		I(anharm)
1(2)	6520.717	6171.471		0
2(2)	6515.109	6227.508		0
3(2)	3273.084	3182.303		0
4(2)	2601.605	2550.816		0
5(2)	2441.469	2395.548		0
6(2)	1868.883	1819.451		0
7(2)	1757.026	1734.234		0
8(2)	1723.632	1691.436		0
9(2)	1574.712	1554.339		0
10(2)	719.745	711.4		0
11(2)	478.277	482		0
12(2)	435.38	435.551		0

Table 6: Anharmonic IR frequencies calculated for Cl 35-35 isotope DCE

for ^{37}Cl-^{37}Cl isotope

Anharmonic Infrared Spectroscopy

Units: Energies (E) in cm^-1

Integrated intensity (I) in km.mol^-1

Fundamental Bands				

Mode(Quanta)	E(harm)	E(anharm)	I(harm)	I(anharm)
1(1)	3260.355	3107.354	0	0.0000727
2(1)	3257.55	3128.986	16.97923504	14.14707324
3(1)	1636.453	1588.661	0	0.00000595
4(1)	1300.735	1276.844	0	0.00000115
5(1)	1220.576	1202.785	20.31970987	16.73000021
6(1)	934.444	912.89	54.44169428	54.01230252
7(1)	875.245	862.474	0	0.00000068
8(1)	855.489	840.735	108.5200055	110.3218605
9(1)	787.239	775.487	0	0.00000295
10(1)	350.924	346.998	0	0.00000002
11(1)	237.41	238.989	3.30738227	3.30465504
12(1)	216.09	215.761	0.20614752	0.22583681
Overtones				

Mode(Quanta)	E(harm)	E(anharm)		I(anharm)
1(2)	6520.709	6171.47		0
2(2)	6515.1	6227.506		0
3(2)	3272.907	3180.546		0
4(2)	2601.47	2550.201		0
5(2)	2441.152	2401.256		0
6(2)	1868.888	1819.254		0
7(2)	1750.491	1728.382		0
8(2)	1710.977	1679.66		0
9(2)	1574.478	1554.092		0
10(2)	701.848	693.626		0
11(2)	474.82	478.618		0
12(2)	432.181	432.413		0

Table 7: Anharmonic IR frequencies calculated for Cl37-37 isotope DCE

for ^{35}Cl-^{37}Cl isotope

Anharmonic Infrared Spectroscopy

Units: Energies (E) in cm^-1

Integrated intensity (I) in km.mol^-1

Fundamental Bands				

Mode(Quanta)	E(harm)	E(anharm)	I(harm)	I(anharm)
1(1)	3260.355	3107.711	0.00000007	0.00764304
2(1)	3257.55	3128.989	16.98185586	14.14898443
3(1)	1636.5	1589.297	0.00007789	0.0002075
4(1)	1300.769	1276.959	0.00005576	0.00002095
5(1)	1220.656	1203.738	20.27106183	18.06810312
6(1)	934.444	912.899	54.4419646	54.0517676
7(1)	877.125	864.262	1.54436934	1.19475029
8(1)	858.417	843.637	107.7991754	109.9660131
9(1)	787.299	775.541	0.00000017	0.00000328
10(1)	355.406	351.397	0.0011884	0.00099695
11(1)	238.272	239.836	3.33175641	3.32986984
12(1)	216.892	216.547	0.2076654	0.22752358
Overtones				

Mode(Quanta)	E(harm)	E(anharm)		I(anharm)
1(2)	6520.71	6171.476		0
2(2)	6515.101	6227.512		0
3(2)	3273	3181.465		0.00000007
4(2)	2601.539	2550.431		0.00000142
5(2)	2441.312	2395.156		0.00000084
6(2)	1868.888	1819.271		0.00000001
7(2)	1754.25	1731.455		0.00927879
8(2)	1716.835	1685.175		0.00667001
9(2)	1574.597	1554.2		0.00000136
10(2)	710.813	702.415		0.00004727
11(2)	476.544	480.313		0.00001026
12(2)	433.783	434.017		0.00004201

Table 8: Anharmonic IR frequencies calculated for Cl35-37 isotope DCE